



TALLINNA TEHNIKAÜLIKOOL
TALLINN UNIVERSITY OF TECHNOLOGY

School of Engineering
Department of Materials and Environmental Technology

INFLUENCE OF pH ON THE PROPERTIES OF CHEMICALLY DEPOSITED CdS THIN FILMS AND SOLAR CELLS

LAHUSE pH MÕJU KEEMILISELT SADESTATUD CdS ÕHUKESTE KILEDE JA
PÄIKESEPATAREIDE OMADUSTELE

MASTER THESIS

Student	Marvin Üürike
Student code	163606 KAKM
Supervisors	Natalia Maticiuc, Nicolae Spalatu
Consultant	Jaan Hiie

Tallinn, 2017

AUTHOR'S DECLARATION

Hereby I declare, that I have written this thesis independently.
No academic degree has been applied for based on this material.
All works, major viewpoints and data of the other authors used in this thesis have been referenced.

“.....” 201.....

Author:
/signature /

Thesis is in accordance with terms and requirements

“.....” 201.....

Supervisor:
/signature/

Accepted for defence

“.....”201... .

Chairman of theses defence commission:
/name and signature/

Table of Contents

INTRODUCTION	9
1 LITERATURE OVERVIEW	11
1.1 Working principle of a solar cell	11
1.2 Thin film solar cells	13
1.2.1 a-Si thin film solar cells	14
1.2.2 CIGS thin film solar cells	15
1.2.3 CdTe solar cells	16
1.3 CBD CdS thin film for CdTe solar cell	18
1.3.1 Impurities incorporated in the CBD process in CdS.....	22
1.4 Summary of literature and aims of the study	24
1.5 Characterization techniques for thin film materials and solar cells.....	25
1.5.1 XRD	25
1.5.2 SEM	27
1.5.3 EDX	28
1.5.4 UV-vis spectroscopy	28
1.5.5 Hall effect and van der Pauw	29
1.5.6 Current-voltage characteristics of solar cells	31
1.5.7 EQE characteristics of solar cells	32
2 EXPERIMENTAL	34
2.1 Fabrication and characterization of CBD CdS and CdS-CdTe solar cells	34
2.1.1 Cleaning of substrates	34
2.1.2 Deposition of CdS thin films by CBD	34
2.1.3 Fabrication of CdS-CdTe solar cell	35
2.1.4 Characterization of CdS thin films and CdS-CdTe solar cells	36
3 RESULTS AND DISCUSSION	37
3.1 Properties of CBD CdS thin films	37

3.2 Properties of CdS/CdTe solar cells.....	43
4 CONCLUSIONS.....	45
ABSTRACT	46
KOKKUVÕTE	47
REFERENCES	48
ACKNOWLEDGEMENTS	52

List of Figures

Figure 1. Formation of p-n junction and occurrence of the internal electric field [19].....	11
Figure 2. Cross section of a thin film solar cell [19].....	12
Figure 3. Evolution of best laboratory efficiencies of different solar cells.....	14
Figure 4. Structure of p-i-n a-Si solar cell [25].....	15
Figure 5. Structure of CIGS solar cell [28].	16
Figure 6. Structure of CdTe solar cell in superstrate configuration (a) and substrate configuration (b).....	17
Figure 7. Traditional setup scheme for CBD technique [45].	19
Figure 8. Scheme of complex decomposition cluster mechanism [46].....	21
Figure 9. Scheme of complex decomposition ion-by-ion mechanism [46].	22
Figure 10. Regions of stability for the Cd/ammonia system for [Cd] = 0.1M and room temperature. Above the hydroxide line Cd(OH) ₂ can exist in the solution, below it cannot. Complex line gives the concentration of free Cd ²⁺ in any given pH value, which is controlled only by ammonia concentration [47].	23
Figure 11. a) Scheme of XRD measurement and b) Bragg's geometry of X-rays reflection. .	26
Figure 12. Scheme of SEM	27
Figure 13. Schematic principle of EDX.	28
Figure 14. Schemes of transmittance and reflectance modes in the UV-vis spectrometry.....	29
Figure 15. Four point probe contact illustration.....	30
Figure 16. Scheme of Hall measurement	30
Figure 17. Ideal diode J-V curves for measurement in the dark and under illumination.....	32
Figure 18. A schematic diagram of idealized EQE curve for CdS-CdTe solar cells [52].....	33
Figure 19. Scheme of vacuum drying setup [45].	35
Figure 20. SEM image of CdS thin film obtained at pH 10.4 for deposition time of 2 hours .	37
Figure 21. SEM surface view (a-d) and cross sectional image (e-h) of CdS thin films deposited for one hour at different pH values: a, e) 8.7 pH; b, f) 9.5 pH; c, g) 10.0 pH; d, h) 10.4 pH.....	38
Figure 22. XRD patterns of CBD CdS thin films deposited at different values of solution pH.	41
Figure 23. Tauc's plots and band gap values of CBD CdS thin film deposited at different pH values of solution.	42
Figure 24. J-V (a) and EQE (b) characteristics of CdS-CdTe solar cells with CBD CdS obtained at different values of solution pH (8.7, 9.5 and 10.0).....	44

List of tables

Table 1: Composition of CBD solution at different pH values	34
Table 2. Thickness, grain size and elemental composition of CBD CdS thin films deposited at different pH values.	40
Table 3. Interplanar distance (d), and lattice parameters (a, c) calculated for the main XRD peak of CdS thin films deposited at different pH values.....	41
Table 4. Electrical properties of CdS thin films obtained at different pH of deposition solution	43
Table 5. Photovoltaic parameters of CdS-CdTe solar cells with CBD CdS film obtained at different values of solution pH (8.7, 9.5, and 10.0)	44

List of abbreviations

a-Si	Amorphous silicon
CBD	Chemical bath deposition
Cd(OH) ₂	Cadmium hydroxide
CdO	Cadmium oxide
CdS	Cadmium sulfide
CdTe	Cadmium telluride
CSS	Close spaced sublimation
EDX	Energy dispersive X-ray spectroscopy
E _g	Band gap
EQE	External quantum efficiency
FF	Fill factor
FTO	Fluorine doped tin oxide
GIGS	Copper indium diselenide
IQE	Internal quantum efficiency
ITO	Indium tin oxide
J _{sc}	Short-circuit current
J-V	Current - voltage
Mo	Molybdenum
SEM	Scanning electron microscopy
TCO	Transparent conductive oxide
TEA	Triethanolamine
TU	Thiourea
V _{oc}	Open circuit voltage
XRD	X-ray diffraction
η	Efficiency

INTRODUCTION

Green energy technologies are under a lot of attention since they are expected to decrease the amount of greenhouse gases emitted to the atmosphere and thus stop or at least slow down one of the biggest environmental problems at the moment which is global warming. Solar energy by the means of thin film solar cells have been recognized as potential future energy source. Research is ongoing for truly low-cost and environment-friendly thin film solar cells with different materials and fabrication technologies.

One of the most important semiconductor materials for the industry of different optoelectronic devices such as optical sensors, light-emitting diodes, transistors and photovoltaic panels has proven to be cadmium sulfide (CdS) [1]. CdS thin films are deposited by several physical and chemical methods such as sputtering [2], vacuum evaporation [3], electrodeposition [4], spray pyrolysis [5], and chemical bath deposition (CBD) [6]. Among them CBD is most widely used in industry as the simplest, fastest, cost effective and promising method to obtain uniform, dense and large area CdS thin films [7], [8].

Due to the aqueous environment of CBD, the CdS film may contain a significant amount of oxygen and hydrogen compounds which influence the growth mechanism and also the thin film properties. This is directly connected to the fact that CBD CdS thin film is obtained from an alkaline solution with a pH value around 10, where the hydroxide mechanism of CdS formation is commonly accepted [8], [9], [10]. The hydroxide ions participate in the decomposition of thiourea with S^{2-} release so that CdS formation occurs preferentially on the surface of hydroxide rather than nucleating separately in the solution. In this sense, the inclusion of $Cd(OH)_2$ in chemically deposited CdS was widely presumed [11], [12], [13], however, its thermal instability [14] and impact on the properties of CdS film were underestimated.

Such unstable thermal activity of hydroxide species generates uncontrollable properties of CBD CdS thin films already at low temperatures [8], [15]. As the OH group incorporates on sulfur site in the CdS lattice [16], it acts as a donor dopant which dramatically changes the electrical, structural and optical properties of CBD CdS thin films already in the deposition process [17]. There is a possibility to remove these OH-containing impurities by means of a post deposition thermal annealing in reducing ambient at temperatures up to 450 °C, but the CdS properties will be also affected [15], [16], [18].

As an alternative, in this master thesis we investigate the possibility to control the incorporation of OH impurities into CdS lattice during the deposition process by changing the

deposition parameters. In this sense we prepare CdS thin films by CBD method at pH values of solution below and above the usual value (pH 10) [8]: 8.7, 9.5, 10.0 and 10.4 pH. In addition, we study the changes followed by the change of pH in crystallography, morphology, elemental composition and also optical and electrical properties of CdS thin films by means of X-ray diffraction (XRD), scanning electron microscopy (SEM), energy-dispersive X-ray analysis (EDX), UV-vis spectrometry, Hall and van der Pauw measurement. CBD CdS thin films deposited at different pH values are used in superstrate CdS-CdTe solar cells and the effect of CBD solution pH on solar cell parameters such as current – voltage characteristics (J-V) and quantum efficiency (QE) is discussed.

This thesis is divided into three main chapters. Following the introduction, the theoretical part includes an overview of photovoltaic effect, different thin film photovoltaic solar cells and materials, chemical bath deposition mechanisms for CdS and also an overview of thin film and solar cell characterization techniques. The experimental part briefly describes the CdS thin film deposition process and fabrication of CdS-CdTe solar cells. The third part is divided into two sections of which the first includes the results and discussions of the properties of CBD CdS thin films and the second shows the results and discussions for obtained CBD CdS application in CdS-CdTe solar cells.

1 LITERATURE OVERVIEW

Photovoltaic solar cells are devices that convert light into electricity using semiconductor materials that exhibit the photovoltaic effect. Due to abundance of solar energy that radiates continuously Earth, these devices offer a prominent solution for becoming independent from fossil fuels as they produce renewable energy with no pollution or greenhouse gases after installation.

1.1 Working principle of a solar cell

Solar cell is a device based on p-n junction which converts radiation from the sun into electricity via photovoltaic effect. The photovoltaic effect is based on two principal mechanisms. First, an electron in the valence band is excited across the band gap by an incident photon of energy, forming an electron-hole pair. The energy of the incident photon must be greater than the band gap of the material for excitation to occur. Then the electron-hole pair must be separated by an electric field to not allow them to recombine. Only then can photocurrent be collected.

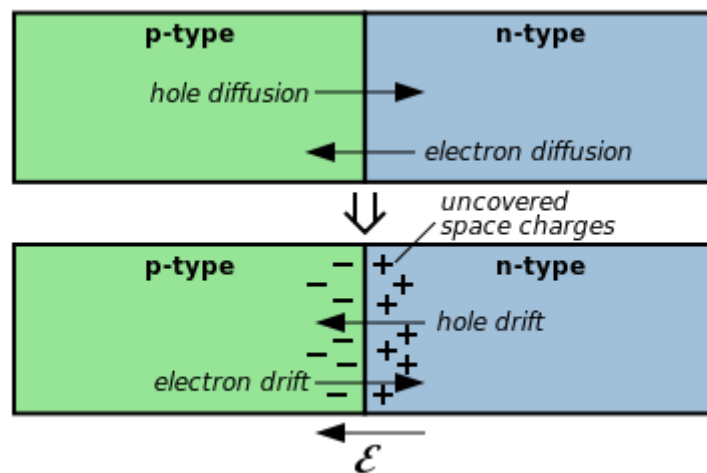


Figure 1. Formation of p-n junction and occurrence of the internal electric field [19].

When p-type and n-type semiconductor materials are brought together a p-n junction is formed (Figure 1). Electrons which are majority carriers in the n-type material diffuse towards p-type material leaving behind holes which are minority carriers. This is sometimes addressed as carriers' diffusion that takes place from the both sides of the junction. Because of the

carriers' diffusion, near the interface of the positively and negatively doped materials the n-type material has a positively charged region with no mobile electrons, whereas the p-type material has minority electrons so it is negatively charged. Thus an electric field is established across the junction that assures the charge separation in the p-n junction [19].

To capture energy from photoelectric effect contacts are put onto the p-type material and n-type material. These contacts are connected with external load, which means that the excited electron recombines with a hole after passing through the external load, thus producing electricity. The general cross section scheme of a thin film solar cell (this thesis deals with thin films only) can be seen in Figure 2.

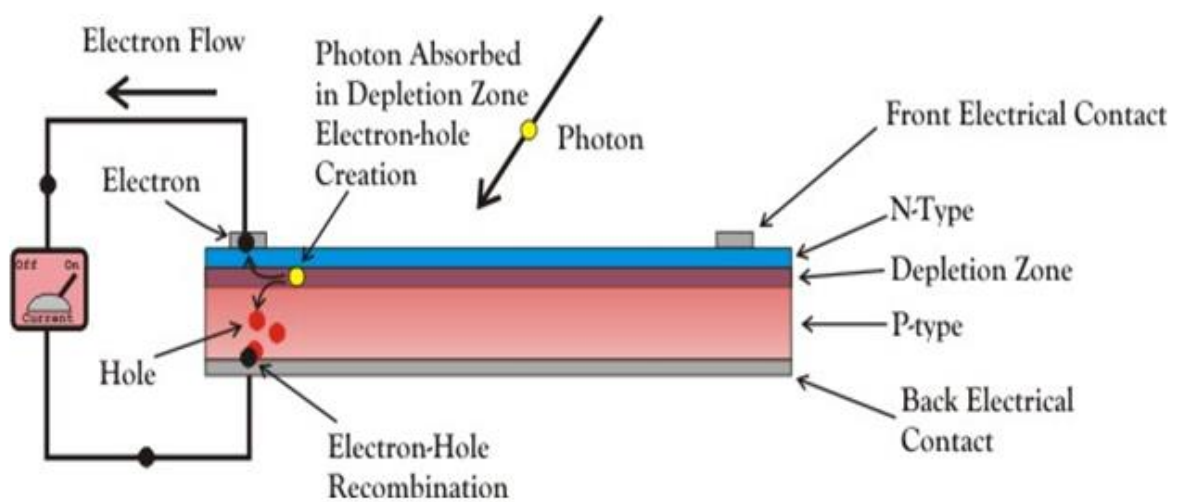


Figure 2. Cross section of a thin film solar cell [19].

The main components of thin film based solar cell are substrate, back contact, p-type material, n-type material and front contact. Regarding the configuration of the cell, there are two types: substrate configuration and superstrate configuration. In superstrate configuration, light enters through the substrate, typically glass, while in the substrate configuration, light enters through the last layer to be deposited. Depending on the configuration type the substrate layers can be transparent or not - glass, metal, ceramic or flexible polymers. Metals such as gold, copper, aluminum or nickel are used as back contacts, as they need to have high conductivity to collect as much possible electric charge. The absorber layer (p-type material) is a positively doped semiconductor with high absorption coefficient. It absorbs light and generates electron-hole pairs. Buffer layer is a negatively doped semiconductor (n-type material) which forms the heart of a solar cell when in contact with the absorber layer – the p-n junction. It is important for the buffer layer to be transparent, conductive and to have a

minimal lattice mismatch with the p-type absorber. Front contact has a similar purpose as the back contact (to collect the electrical charge and transport it to the external circuit) but it also has to be transparent in order to let the light reach the p-n junction interface. Transparent conductive oxides (TCO) such as fluorine doped tin oxide (FTO), zinc oxide or indium tin oxide (ITO) are used as front contact for solar cells.

There are so called three generations of solar cells based on technology. The first generation solar cells are mainly based on silicon wafers and their efficiency is about 15 - 20 %. First generation solar cells have dominant market position and have decent performance and are stable, however they are rigid and require a lot of energy in production. The second generation solar cells are based on amorphous silicon, CIGS and CdTe – they have typical efficiencies around 10 – 15 %. The production cost has gone down in the case of second generation solar cells due to lower material consumption than first generation solar cells. Also second generation solar cells have good stability and can be produced in a manner that they are flexible. Since production still uses high temperatures and vacuum processes, high energy consumption of production is associated to second generation as well as first generation solar cells. For third generation solar cells organic materials and polymers are used for solar cell fabrication. These types of solar cells have very little commercial application because of their very high production cost. The performance and stability of third generation solar cells is still very poor comparing to first and second generation solar cells. Second generation, also called thin film solar cells are more efficient in terms of energy, price and stability thus thin film solar cells are discussed in this work [20].

1.2 Thin film solar cells

Thin film solar cells, also known as second generation solar cells have attracted worldwide research attention over the past three decades due to potential lower manufacturing costs and minimal material consumption comparing to classical crystalline silicone solar cells or first generation solar cells.

There are three main groups of thin film solar cells: amorphous silicon (a-Si), copper indium gallium diselenide (GIGS) and cadmium telluride (CdTe) solar cells. Thin film solar cells have record efficiencies of 22,3% for GIGS [21], 21,5% for CdTe [22] and 13,4% for a-Si [23]. Best lab efficiencies of various solar cells obtained by different groups are mapped in Figure 3.

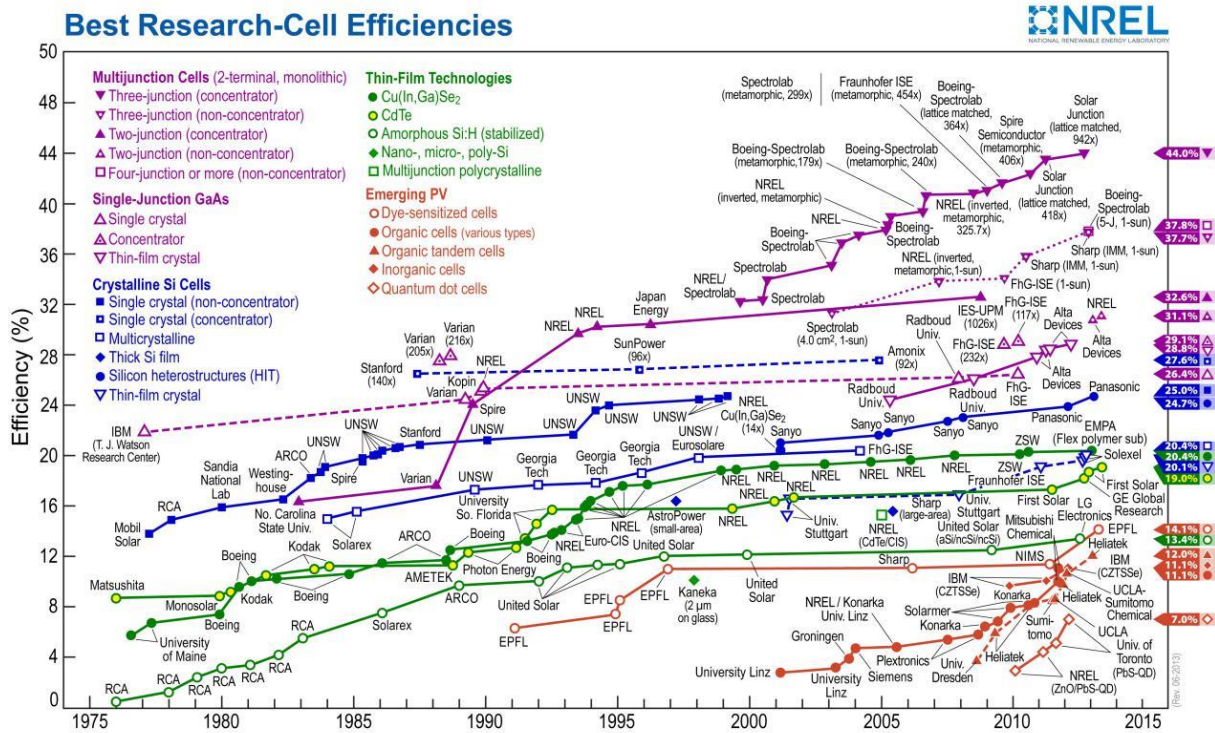


Figure 3. Evolution of best laboratory efficiencies of different solar cells.

1.2.1 a-Si thin film solar cells

a-Si represents an attractive material for solar cells due to its abundance and non-toxicity. Thin film a-Si solar module has lower manufacturing costs than crystalline silicon solar cell as it requires a lower processing temperature and enables a scalable production upon flexible and low-cost substrates with little silicon material required [24]. a-Si solar cell can be made in two different configurations: the superstrate configuration ('p-i-n') or the substrate configuration ('n-i-p') in accordance with the sequence of layers.

In a-Si cell the p-i-n photodiode configuration is more widely employed because of efficient collection of photogenerated carriers in the presence of an electric field (Figure 4).

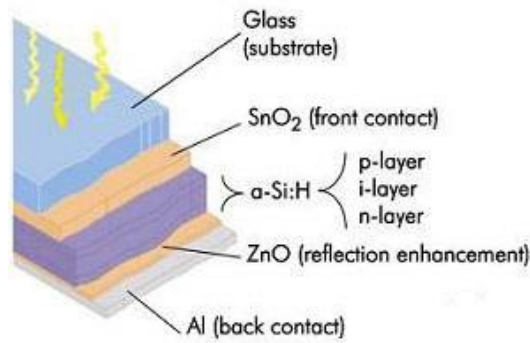


Figure 4. Structure of p-i-n a-Si solar cell [25].

Besides the above mentioned advantages of a-Si solar cell, low efficiency and degradation issues make it hard to compete with other thin film solar cell. Efficiency of a-Si solar cells under light exposure degrades with time – the so called Staebler-Wronski effect. Due to this effect the dark current and photoconductivity of hydrogenated a-Si is reduced significantly by prolonged illumination with intense light. However, on heating the samples to above 150 °C, a-Si solar cells could reverse this effect [26].

1.2.2 CIGS thin film solar cells

Another category of thin film solar cells are made with a thin absorber layer of CIGS. Due to high absorption coefficient of CIGS material with a suitable band gap (from 1.1 to 1.7 eV) [27], a much thinner film is required compared to other semiconductor materials. CIGS layers are thin enough to be flexible, allowing them to be deposited on flexible substrates. However, as all of these technologies normally use high-temperature deposition techniques, the best performance normally comes from cells deposited on glass. The common device structure for CIGS solar cells is shown in Figure 5.

The glass substrate is typically soda lime glass due to the fact that the sodium diffuses into the CIGS layer increasing the conductivity and reducing the formation of lattice defects [24]. Molybdenum (Mo) is used as a back contact as it can tolerate the harsh reactive ambient of the selenization process at high temperature and form an ohmic contact with CIGS. The CIGS absorber layer is deposited onto Mo back contact after which a thin CdS layer is deposited onto CIGS layer. CdS is the buffer layer of this cell and has a direct band gap of 2.4 eV. A high resistance and low resistance bilayer of i-ZnO/ZnO:Al is sputtered onto the cell as transparent conductive oxides. Finally, nickel/aluminum (Ni/Al) grid contacts are added for energy flow (Figure 5).

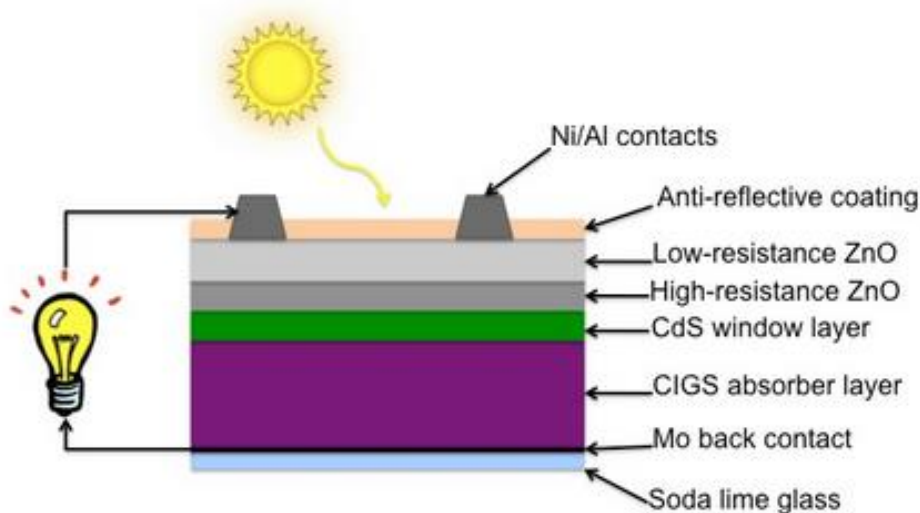


Figure 5. Structure of CIGS solar cell [28].

Although CIGS based solar cell have a very high potential to reduce production costs for photovoltaic modules, the translation of laboratory results to large scale manufacturing has been much more difficult than expected due to the complexity of the processes involved for making CIGS thin film PV modules [29]. The design, operation and control of commercial scale equipment required for the deposition of the CIGS need to be custom designed, with little or no previous technology to draw upon. Due to Na incorporation (diffusion of Na from the glass substrate) a variation in performance can be caused across the module [24]. The thickness of the buffer layer is usually less than 50 nm and is difficult to be controlled across the textured surface of the CIGS, low V_{oc} resulting in increased area loss.

1.2.3 CdTe solar cells

CdTe thin film solar cells are very similar to CIGS solar cells. CdTe has a direct band gap of 1.45 eV and it is used as the absorber layer material. The basic device structure is shown in Figure 6. For substrate configuration cells, the main advantage is that the substrate does not have to be transparent, which allows a variety of foils (e.g., molybdenum, stainless steel or polyamide) as a substrate for the development of flexible cells [30]. The highest efficiency for CdTe solar cells, however, was achieved in the superstrate configuration.

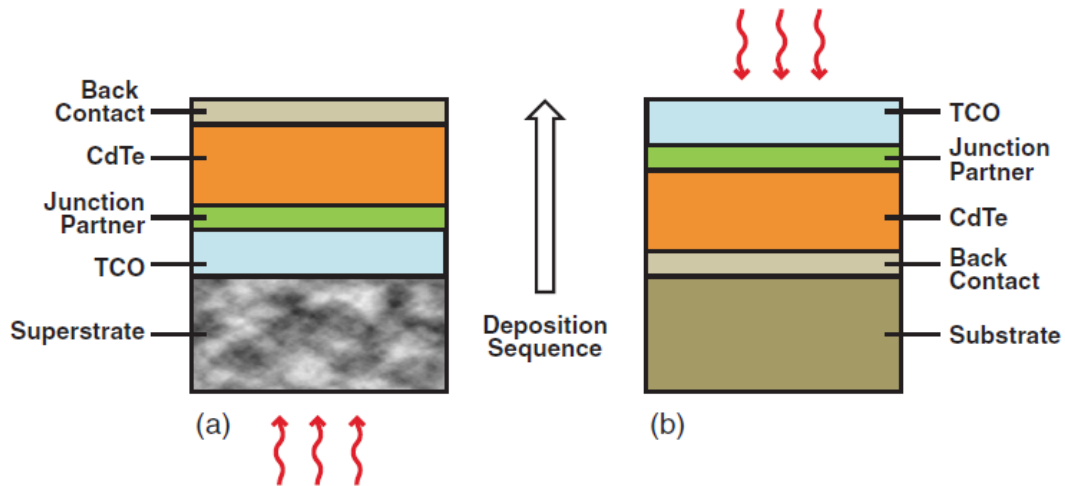


Figure 6. Structure of CdTe solar cell in superstrate configuration (a) and substrate configuration (b).

The CdS/CdTe layers for superstrate configuration cells are grown on glass substrates coated with TCO. The glass substrate can be a low-cost soda-lime glass for growth process temperatures below 550 °C, or alkali-free glass for high-temperature processes (550–600 °C). Various back contacts can be applied, as they do not have to withstand the high temperature of successive layer deposition. Typical process steps for fabricating a CdS/CdTe solar cell with superstrate configuration include deposition of a TCO layer, CdS buffer layer and CdTe absorber layer followed by postdeposition procedures such as CdCl₂ heat treatment and etching of the CdTe film surface. The last step of fabrication is evaporation of a back contact. The lab efficiency of CdTe thin film cells in superstrate configuration has increased significantly in recent years reaching recently a conversion efficiency of 21.5 % [22].

The advantages of CdS/CdTe solar cell are connected with the fact that CdTe is a robust semiconducting material, which can be prepared by various synthetic routes in a highly reproducible manner and its remarkable tolerance towards high processing temperatures makes it ideal for large scale industrial production. In addition CdTe is a good absorber material for solar cell due to its ideal bandgap of ~1.5 eV and its high optical absorption coefficient $>5 \times 10^5 \text{ cm}^{-1}$. Therefore, more than 90% of the incident light is absorbed in a few micrometers of the material [31]. Another advantage of CdTe is its compatibility with n-type CdS, which is a wide-band-gap semiconductor (~ 2.4 eV) for which it is a good transparent to the bulk of solar radiation. Typically, the CdS layer is made as thin as possible to allow the maximum number of photons to pass through to the CdTe layer. These two polycrystalline materials (CdTe and CdS) are chemically stable and high optical quality layers are deposited in the temperature range of 400– 600°C. Since high thermal treatment is involved during CdTe deposition by most of the preparative techniques, CdTe films are associated with V_{Cd}

giving rise to p-type conductivity. The high ionicity (72%) of CdTe results in well-passivated crystallites, while high chemical and thermal stability is associated with strong chemical bonding (5.75 eV) [32]. The stability region of CdTe is extremely narrow (2×10^{-6} at.% wide) and is symmetrical with a perfect stoichiometry at 400°C [33]. CdCl₂ air treated CdTe at 420 °C will have a p-type carrier concentration $>10^{14} \text{ cm}^{-3}$ to form a junction with its n-type partner [34].

Another important aspect of CdTe is that the carrier lifetime for CdTe is small (of the order of 10^{-7} s) with a mobility ranging from 10 to 100 $\text{cm}^2 \text{ V}^{-1} \text{ s}^{-1}$. The short optical absorption length in II–VI compounds also renders the carrier diffusion length in minority carrier devices relatively insignificant. The diffusion length in CdTe film grains will be between 1 and 5 μm and hence the active layer thickness will be within the limits of 1–5 μm [35]. The reduced thickness of the absorber gives rise to an intense electric field and therefore a large fraction of carriers will be generated within the depletion layer, facilitating efficient carrier collection [36].

CdS is the most widely used buffer material for thin film CdTe solar cells due to its direct optical band gap of 2.4 eV and high transparency (>80%). For such application CdS film should be conductive ($n \sim 10^{16} \text{ cm}^{-3}$) and thin enough to allow high transmission in the range of 50–100 nm. Thinning increases the transparency of CdS film and gains in short-circuit current while the uniformity of the film avoids the short circuit effects between transparent conductive oxide and CdTe absorber. CdS as the buffer layer for CdTe solar cell also facilitates the formation of large bandgap CdTe_{1-x}S_x mixed crystal layers near the CdS/CdTe interface, which decreases the lattice mismatch and the amount of interface defects. [37] [38].

1.3 CBD CdS thin film for CdTe solar cell

CdS is a bright yellow/orange solid substance with a solubility product of 10^{-28} . In nature it is found in both zinc blende and in wurtzite forms.

CdS is a wide band gap prominent semiconductor with diverse range of applications such as field effect transistors [39], photocatalysis [40] and buffer layer in photovoltaic conversion [41]. The band gap of the semiconductor is approximately 2.45 eV [42], which corresponds to the green light in visible wavelength spectrum making it useful in detecting visible radiation.

There are numerous deposition techniques for obtaining thin film CdS such as vacuum evaporation and subsequent cadmium chloride treatment [3], CBD [6], spray pyrolysis [5], pulsed laser deposition [43], sputtering [2] and electrodeposition [4].

By far the simplest method for obtaining thin films is CBD, all that is needed is a vessel, a dilute aqueous solution of common chemicals and a substrate onto which deposition occurs. A magnetic stirrer for agitation of the solution and a thermostated bath are usually a part of the experimental setup (Figure 7). CBD CdS is also a cost effective and promising technique to obtain thin films with high transparency, low dark electrical resistivity, high photoconductivity, better crystallinity, and uniform coverage of the substrate [44].

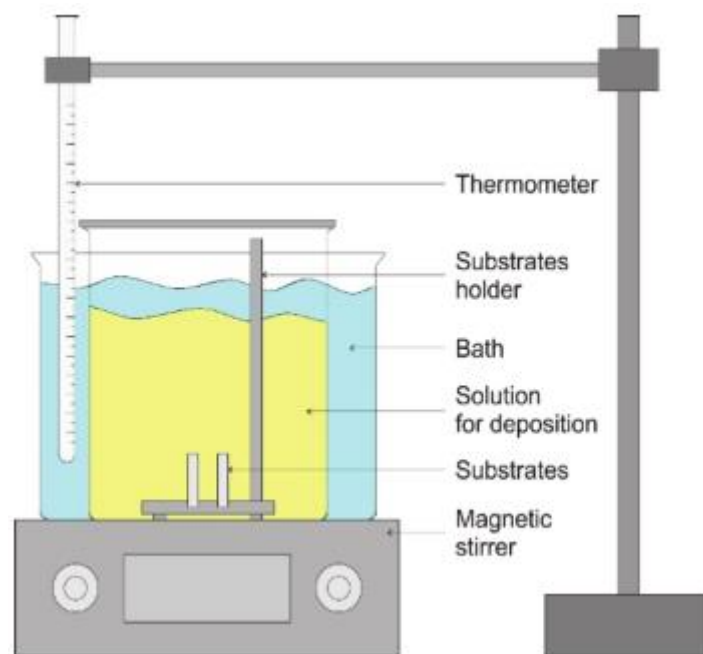


Figure 7. Traditional setup scheme for CBD technique [45].

CBD represents a deposition of films on a solid substrate as a result of a reaction in an (almost always) aqueous solution. For example, if Cd salt and sulfide ions are introduced in the solution, CdS will precipitate immediately. These precipitated particles in the solution in the purpose of obtaining thin film would be unwanted. During CBD, the reaction rate is controlled to be slow enough to allow CdS to form gradually on the substrate ultimately giving a semiconductor thin film. The reaction rate can be controlled by the concentration of sulfide-precursor the temperature and the pH of the solution. The sulfide-precursor (often thiourea) is responsible of slow sulfide ion generation in the solution. For most CBD solution the pH is in the alkaline region. This is important for hydrolysis of thiourea as sulfide

generating reaction. To prevent metal hydroxides from precipitation, complexing agents are added. [8]

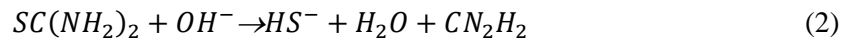
The reaction mechanism of the CBD can be divided into two main processes. With the assumption of free ions being present in the solution, there is ionic reaction to produce required compound. Decomposition of metal complexes is another mechanism for wanted compound production. Hodes suggests four main reaction mechanisms for CdS CBD:

1. Ion-by-ion mechanism
2. Cluster mechanism
3. Complex decomposition cluster mechanism.
4. Complex decomposition ion-by-ion mechanism [8]

Ion – by – ion mechanism is considered to be the simplest. It is illustrated with equation (1).

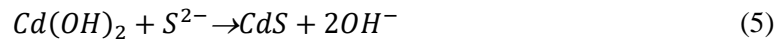


CdS can form as a solid phase, when $[Cd^{2+}][S^{2-}]$ exceeds the solubility product of CdS. Needed sulfide anion comes from the thiourea hydrolysis, equations (2). and (3).



In principal, the sulfide ion generation reaction rate can be easily controlled by temperature or pH, which means the deposition rate, even at high Cd cation concentrations, should be easily controlled as well. Since the reaction is carried out in an alkaline solution a complexing agent is needed to keep Cd cation in the solution and prevent it from precipitating as hydroxide. Ammonia can be used as a suitable complexing agent, which also makes the solution alkaline that is needed for thiourea hydrolysis. [8]

The cluster mechanism is based on sulfide ion replacing hydroxide group in cadmium hydroxide. Following equations (4) and (5) illustrate the cluster mechanism reactions.



The reason equation (5) happens is due to the fact that the solubility product of cadmium sulfide is much less than cadmium hydroxide, therefore reaction is thermodynamically favored. It is found, that solid cadmium hydroxide is formed (4) on substrate with lower pH values than in bulk, meaning it forms onto substrate with lower hydroxide anion concentrations than dictated by the solubility product. Also it has been found that precipitation with conditions allowing precipitation only on substrate (not in bulk) gives

better quality films (more adherent and specularly reflecting) than with precipitation in bulk. [8]

Complex decomposition cluster mechanism is based on the complex formation. Sulfide donor molecule forms a complex with previously precipitated cadmium source. The complex decomposes leaving solid phase adhered CdS on substrate. Reaction is illustrated with equations (6), (7) and in Figure 8.

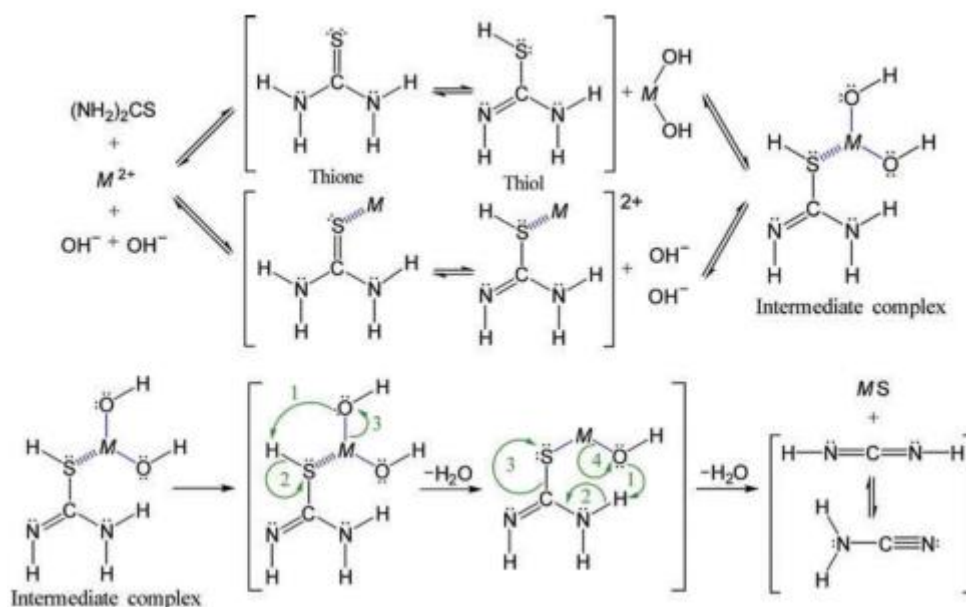
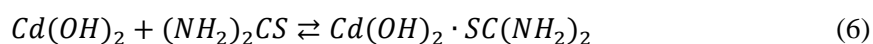
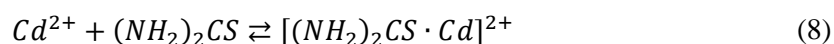


Figure 8. Scheme of complex decomposition cluster mechanism [46].

The complex seen in equation (6) can be formed with different possible ligands based on the solution for example ammine ligands. [8]

Complex decomposition ion – by – ion mechanism is based on ion – complex formation. Cadmium cation may complex with thiourea giving Cd-thiourea complex cation. This complex could hydrolyze by breaking the C-S bond forming CdS. It can happen in bulk solution when complex is formed in bulk and on substrate if cadmium cation is previously adsorbed on substrate. Preferably adsorbed complex is conditioned for good quality film. This mechanism is illustrated with equations (8), (9) and in Figure 9.



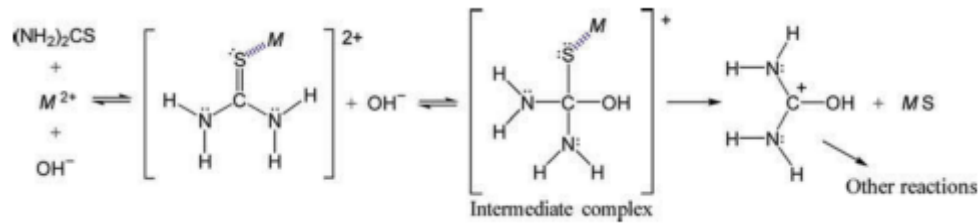
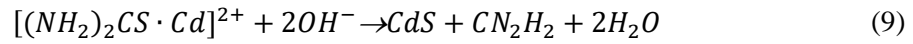


Figure 9. Scheme of complex decomposition ion-by-ion mechanism [46].

It is important to note, that one mechanism does not cancel another, therefore all mechanisms can occur simultaneously, in a sequence or one at a time, depending on the deposition parameters. Since most of chemical reactions are in fact equilibrium reactions, some tendencies in which reaction mechanism is dominant can be derived [8].

Despite the experimental simplicity of CBD and the long history of CdS research, there is still incomplete understanding of the reaction mechanisms and ability to control the film composition and other properties of CdS for device applications.

1.3.1 Impurities incorporated in the CBD process in CdS

The participation of $Cd(OH)_2$ in the CdS formation cannot happen unless it is able to form in the solution. Kitaev et al. presented a theoretical thermodynamic treatment of Cd^{2+} /ammonia/thiourea system to show when $Cd(OH)_2$ should be present in the deposition solution of CdS. The graphical representation of this analysis is shown in Figure 10. This graph is based on $Cd(OH)_2$ solubility product equilibria and the stability constant of the ammine complex of Cd [47].

Considering both hydroxide and complex lines on Figure 10 it can be suggested that on the left side, where complex line is above the hydroxide line, the concentration of free Cd^{2+} will be high enough to form $Cd(OH)_2$. Similarly, on the right side from where the lines cross, $Cd(OH)_2$ will form only if additional alkaline (not ammonia) is added to the solution for extra OH^- ions [47].

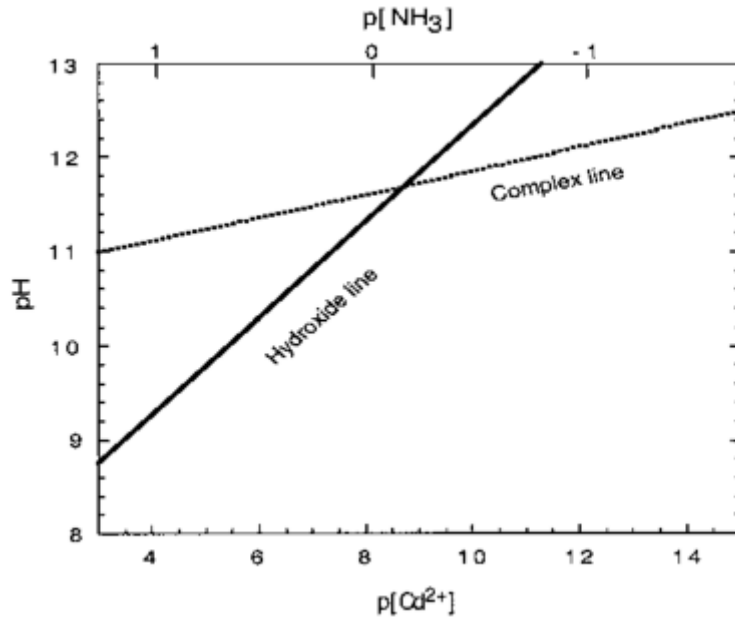


Figure 10. Regions of stability for the Cd/ammonia system for $[Cd] = 0.1M$ and room temperature. Above the hydroxide line $Cd(OH)_2$ can exist in the solution, below it cannot. Complex line gives the concentration of free Cd^{2+} in any given pH value, which is controlled only by ammonia concentration [47].

Independent on deposition parameters and post - deposition treatments there are still impurities left in the CdS lattice that can affect the properties of semiconductor film [8].

Nitrogen (up to 5 atomic %) occurs probably mainly as cyanamide, although other C-N bonded compounds such as cyanide were also believed to be present. These compounds can adsorb to Cd or even to CdS moiety. Nitrogen impurities can be reduced by reducing the concentration of thiourea in the bath to almost zero. Most of nitrogen impurities can also be removed in dissolution of water at $60\text{ }^\circ\text{C}$ [37].

Still the main impurity in the chemically deposited CdS thin films is oxygen (up to 11 atomic %) [8], which can appear in many proposed forms such as carbonate, adsorbed water, surface sulfate, decomposition products of thiourea, cadmium oxide and cadmium hydroxide [8]. Carbonate could come from dissolved atmospheric CO_2 and from decomposition of thiourea whereas $Cd(OH)_2$ is more likely to form when pH is high or ammonia concentration is low. It is important to note that for thin film CdS about 10% of the atoms will be located at a crystal surface, meaning adsorption of oxygen or water would already show a relatively large amount of oxygen content. However, if this oxygen does not substitute sulfur atom, the Cd:S ration would remain the same. If oxygen from other sources (not adsorbed) substitutes the sulfur in the lattice, the Cd:S ratio would be increased. Oxygen impurities can be

successfully removed from CBD CdS thin films by a rapid thermal annealing in vacuum or a reducing atmosphere [48], [8].

To reduce the amount of oxygen impurities in CdS lattice, a post – deposition thermal treatment in reducing ambient can be used [18]. Another way to manipulate the oxygen impurity content in CBD CdS is through the parameters of the deposition process. One of these controllable parameters is the solution pH. Tuning the values of solution pH would allow controlling the amount of hydroxides that participate in the complex decomposition of clusters mechanism which is usually responsible for the CdS growth from an alkaline solution.

1.4 Summary of literature and aims of the study

The studies reported in the literature on the CBD CdS thin films and its application on solar cells can be summarized as follows:

1. CdS is an interesting II-VI compound semiconductor in the field of material science due to its properties, such as wide band gap, high transparency, tunable n-type electrical properties, the ability to have a zinc blende or wurtzite structure and the numerous available fabrication techniques.
2. One of the most important applications of CdS is in the fabrication of solar cells. CdS is considered as a n-type buffer for CdTe, CIGS and kesterite absorbers in superstrate or substrate configurations.
3. The major advantages for CBD CdS can be listed as follows: large area deposition, conformal coating, controllable thickness and compatibility with a variety of applicable substrates.
4. As deposited CBD CdS films tend to form in the cubic phase and have good crystalline quality. Also these films may contain numerous adherent particulates of homogeneously nucleated CdS and a high concentration of impurities, which endows the layers with a high speed of recrystallization at low processing temperatures.
5. The effect of thermal annealing in different conditions on the properties of CBD CdS thin films has been widely investigated. Thermal annealing improves the film crystallinity, changes the E_g , supports the phase transition and changes electrical properties. The changes in the properties were connected with the presence of OH impurities in the thin film.

6. Although thermal annealing of CBD CdS is widely investigated, there are less studies about the effect of CBD solution pH on the properties of CdS and fabricated solar cells. Also there is absence of unified description of physico-chemical processes influenced by pH in solution.

Based on the literature overview, this thesis has the following aims:

1. To get acquainted with the CBD method and to prepare CdS thin films by this method;
2. To investigate the possibilities to change the pH of the CBD solution by changing the concentration of ammonia in the deposition bath;
3. To study the effect of pH of the deposition solution on the microstructural, crystallographic, optical and electrical properties of CBD CdS thin films – a special interest was paid to the presence of OH impurities incorporated in the CdS lattice;
4. To describe the role of solution pH on the physico-chemistry of the CdS thin film growth processes in deposition solution.
5. To apply the CBD CdS thin films deposited at different pH in superstrate CdS-CdTe solar cells and follow the changes in their properties.

1.5 Characterization techniques for thin film materials and solar cells

For characterization of thin film properties various techniques can be used. In this work we investigated the phase composition and crystallographic properties of CdS thin films by means of X-ray diffraction (XRD). The morphology, coverage, grain size and thickness was studied by using scanning electron microscopy (SEM) while for the analysis of local elemental composition energy dispersive X-ray spectroscopy (EDX) was used. For the analysis of optical characteristics a UV-vis spectroscopy was applied. Finally, for the investigation of electrical properties of CdS thin films Hall effect and van der Pauw techniques were applied. For solar cell characterization the classical current-voltage and external quantum efficiency (EQE) characteristics were measured under AM 1.5 conditions in order to obtain the main photovoltaic parameters of CdS-CdTe solar cells.

1.5.1 XRD

XRD measurements are conducted to determine phase composition and crystallographic properties of thin films. On the basis of XRD measurements lays the classical

electromagnetic theory when an electron is oscillating in alternating electromagnetic field with the same frequency as the field. When an X-ray beam hits the atom, electrons of that atom will oscillate in the frequency of the beam. An accelerated charge emits electromagnetic radiation. In most cases the emitted radiation interferes destructively, however in the right angle of radiation the emitted radiation coincides and leave the crystal. Diffraction of X-rays is described by Bragg's equation (10).

$$n\lambda = 2d \cdot \sin\theta \quad (10)$$

where λ is X-ray wavelength, d is interplanar distance, θ is angle of incidence with lattice plane and n is integer.

X-rays with constant wavelength are radiated towards crystal lattice, radiation reflects from lattice atoms illustrated (Figure 11), which is captured by detector. [49]

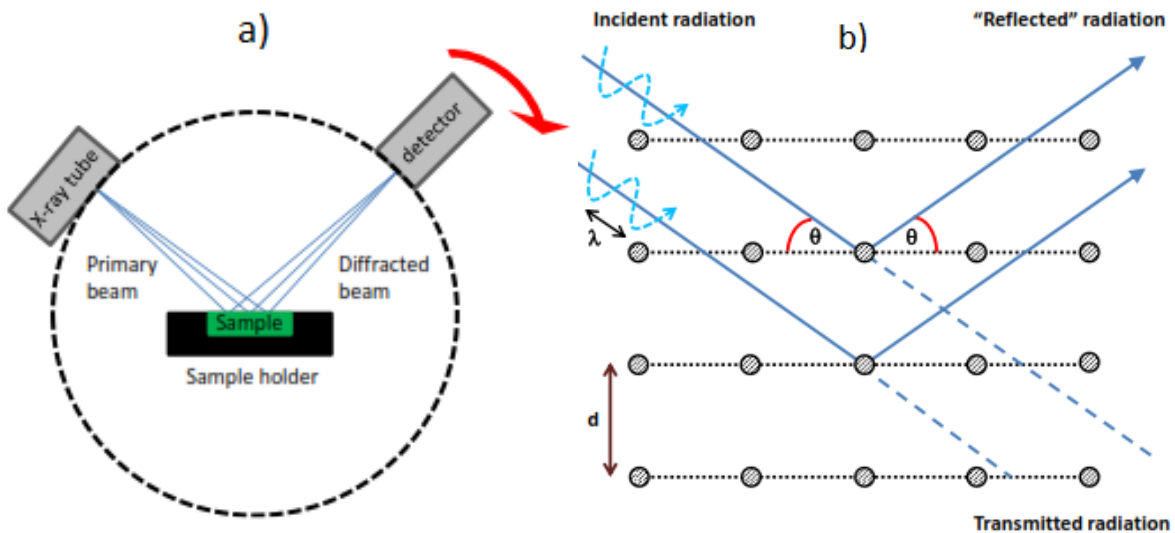


Figure 11. a) Scheme of XRD measurement and b) Bragg's geometry of X-rays reflection.

The intensity of detected radiation is plotted against 2θ . As it is seen (Figure 11b) the angle of radiation is varied to find angles where Bragg's equation (10) is satisfied. These angles will generate diffraction peaks in the XRD pattern and these peaks can be compared with previous experimental data giving us information of phase composition, lattice parameters and crystallites orientation. Additionally, the crystallite size can be calculated by Scherrer equation (11).

$$B(2\theta) = \frac{K\lambda}{L \cos\theta} \quad (11),$$

where L is the crystallite size, B is the peak width, K is the Scherrer constant, λ is the wavelength of X-radiation θ is the half of the diffraction angle.

1.5.2 SEM

SEM analysis gives a good insight of thin film morphology, coverage, grain size and thickness. SEM takes advantage of secondary electrons emission when they bombard the investigated thin film. Bombarding electrons are created in an electron gun by heating or applying a strong electric field to filament. An anode will accelerate the electrons down the column towards the sample (Figure 12). Magnetic lenses focus the resulting electron beam with a diameter down to 1 nm onto the sample [49].

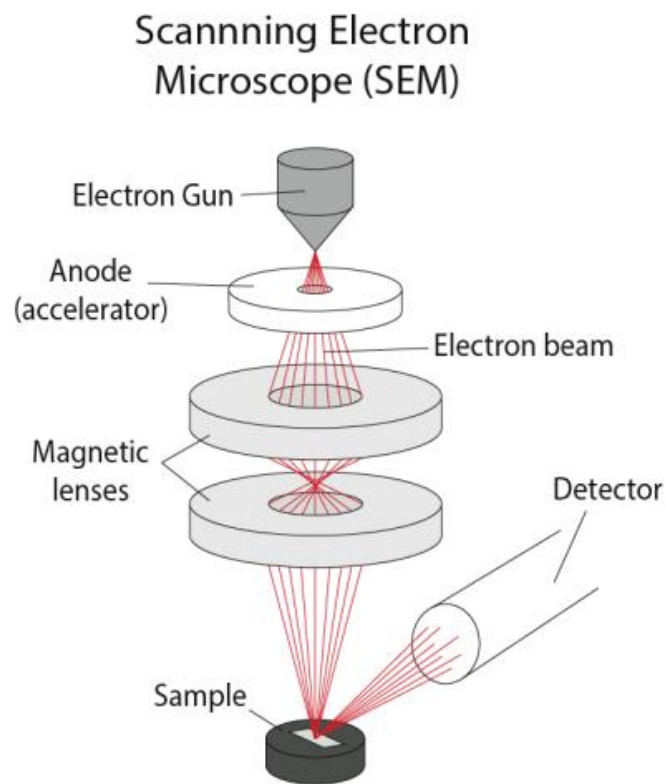


Figure 12. Scheme of SEM

The amount of secondary emitted electrons depends, among other things, on sample topography. These secondary electrons can be detected with a positively charged detector outside microscope column and as they are emitted at the surface of the sample it gives topological information and an image of the surface is created.

1.5.3 EDX

Very often SEM instruments are equipped with EDX detectors that are used to analyze the local elemental composition of thin films. Electrons are able to interact with atom's inner shell electrons in a way that results the inner shell electron exiting from atom's electron cloud. During this action holes are left behind giving second shell electrons a possibility to fill them. If this occurs, the difference of outer shell and inner shell electron potential energy can be emitted as X-ray quantum or as Auger electron. The emitted X-ray quantum energy is element specific, giving this way a possibility to analyze the chemical composition of the measured material. The principal scheme can be seen on Figure 13.

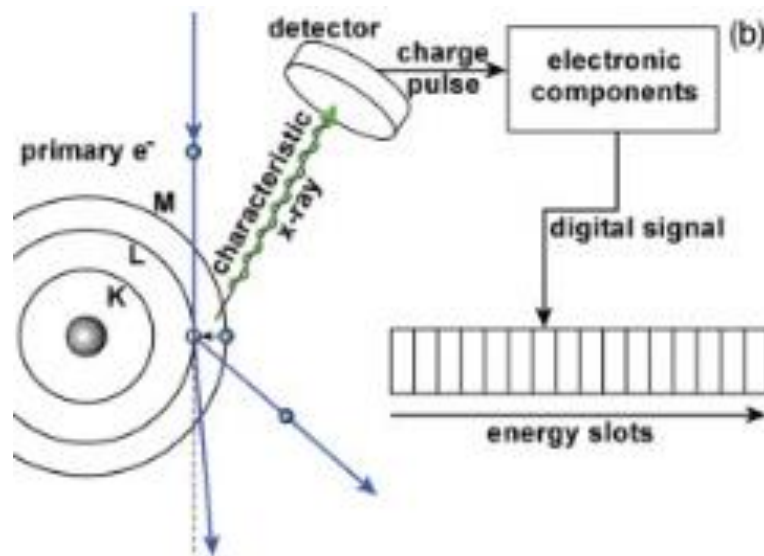


Figure 13. Schematic principle of EDX.

1.5.4 UV-vis spectroscopy

UV-vis spectrometry is applied to describe thin film optical characteristics such as transmittance, reflectance and absorbance which also allow determining the thickness, the absorption coefficient and the band gap of the film. Transmittance and reflectance spectra are measured inside an integrated sphere which scheme can be seen in Figure 14.

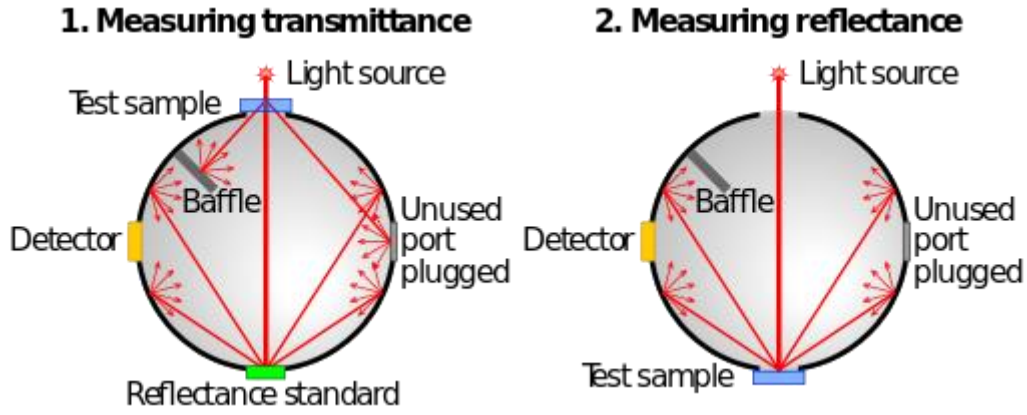


Figure 14. Schemes of transmittance and reflectance modes in the UV-vis spectrometry.

Transmittance and reflectance spectra are obtained by dividing transmitted or reflected light to the incident light. Based on these spectra the absorption coefficient, α , can be calculated by means of equation (12).

$$\frac{T}{100 - R} = e^{-\alpha d} \quad (12),$$

where d is the thickness of the film.

The optical band gap is evaluated from the Tauc's relation between E_g and derived absorption coefficient (13).

$$(\alpha h\nu)^n = A(h\nu - E_g) \quad (13),$$

where A is a constant, h is Planck's constant, ν is light frequency. The value of n number is 2 for direct transitions and 0.5 for indirect transitions. The linear part of a plot of $(\alpha h\nu)^2$ against photon energy ($h\nu$) is extrapolated to x-axis, giving the value of (E_g) [50].

1.5.5 Hall effect and van der Pauw

Van der Pauw or four point probe technique can be used to measure sheet resistance of a film. Knowing thickness of the sample the electrical resistivity can be also calculated. For the measurement procedure four points are chosen in the corners of a square in a fashion shown in Figure 15.

The measurement is based on a relation seen in equation (14).

$$\exp\left(-\frac{\pi d}{\rho} R_A\right) + \exp\left(-\frac{\pi d}{\rho} R_B\right) = 1 \quad (14),$$

where d is the thickness of the thin film, ρ is the resistivity of the material, whereas R_A and R_B are sheet resistances (Figure 15) [51].

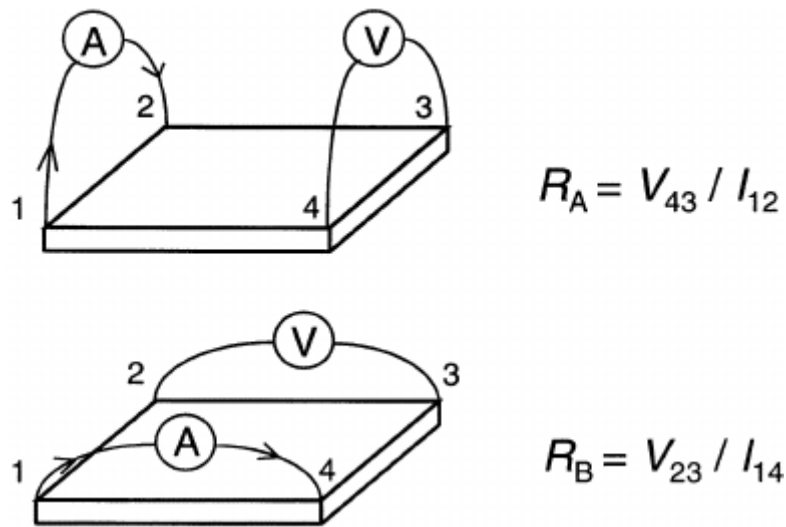


Figure 15. Four point probe contact illustration.

The Hall effect is due to the nature of the current in a conductor which consists of the moving charge carriers, typically electrons, holes, ions or all three move in a straight line. When a magnetic field is present, these charges experience a force, called the Lorentz force, which curve the paths of charge carriers in a manner that moving charges accumulate on one face of the material (Figure 16). This leaves equal and opposite charges exposed on the other face, where there is a scarcity of mobile charges establishing an electric field.

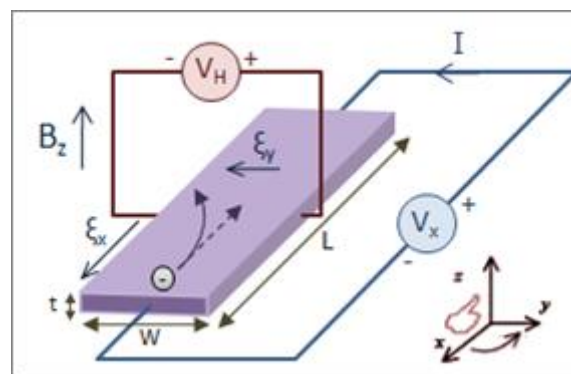


Figure 16. Scheme of Hall measurement

$$R_H = \frac{E_y}{j_x B} = \frac{V_H t}{IB} = -\frac{1}{ne} \quad (15)$$

In equation (15) R_H is the Hall coefficient, E_y is the induced electric field, j_x is current density, B is the Boltzmann constant, V_H is the voltage, I is the current, n is the number of charge carriers and e is the charge of each carrier.

As a result, the Hall effect is very useful as a means to measure either the carrier density or the magnetic field.

1.5.6 Current-voltage characteristics of solar cells

To characterize a solar cell, standard device performance parameters such as open circuit voltage (V_{OC}), short circuit current density (J_{SC}), fill factor (FF) and efficiency are used. These parameters are extracted from the graphical representation of Shockley diode equation (16),

$$J = J_0 \left(e^{\frac{qV}{AkT}} - 1 \right) \quad (16),$$

where J is the diode current density, J_0 is the reverse saturation current density, q is the electron charge, V is the voltage, A is the diode ideality factor, k is Boltzmann's constant, and T is the temperature. When device is placed under a light source a light generated current density term (J_L) is added to the equation (17).

$$J = J_0 \left(e^{\frac{qV}{AkT}} - 1 \right) - J_L \quad (17)$$

J-V curves for an ideal device in dark or under illumination are represented in Figure 17. [19]. Based on these dependencies the photovoltaic parameters of the solar cell can be determined.

J_{SC} is the current generated by the device under no applied bias ($V=0$) and is determined as the y-intercept of the light J-V curve in Figure 17.

V_{OC} is defined as the applied bias at which no current flows through the device and is determined from the x-intercept of the light J-V curve in Figure 17. The V_{OC} can be also determined from equation (17) by setting the condition that $J=0$.

$$V_{OC} = \frac{Akt}{q} \ln \left(\frac{J_L}{J_0} + 1 \right) \quad (18)$$

It is clear that V_{OC} is a function of dark as well as light generated current density terms (18).

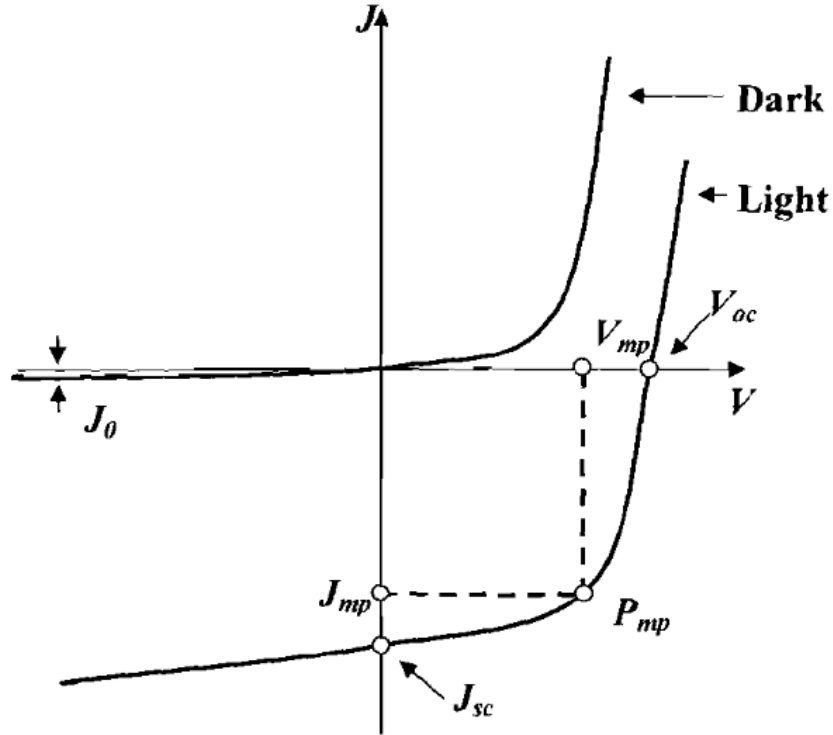


Figure 17. Ideal diode J-V curves for measurement in the dark and under illumination

The fill factor is a measure of the “squareness” of the curve with higher values tending towards a square response and lower values tending towards a straight line. The fill factor is defined as a ratio of the size of the maximum power rectangle to the rectangle formed by the product of the short current density and open circuit voltage, which can be calculated with the following equation:

$$FF = \frac{P_{mp}}{J_{sc}V_{oc}} = \frac{J_{mp}V_{mp}}{J_{sc}V_{oc}} \quad (19)$$

Device efficiency (η) is defined as the ratio of the maximum power generated by the device (P_{mp}), to the power of the radiation incident upon it (P_s) and is calculated as follows:

$$\eta = \frac{P_{mp}}{P_s} = \frac{(V_{oc}J_{sc}FF)}{P_s} \quad (20)$$

1.5.7 EQE characteristics of solar cells

The QE measurement is an indicator of how good the solar cell is at converting sun light to electricity. A solar cell should optimally have high spectral response at the point at which the spectral component of the sunlight is abundant. Quantum efficiency is the ratio of the number of charge carriers that are collected by the solar cell to the number of photons of a given wavelength shining on the solar cell (Figure 18).

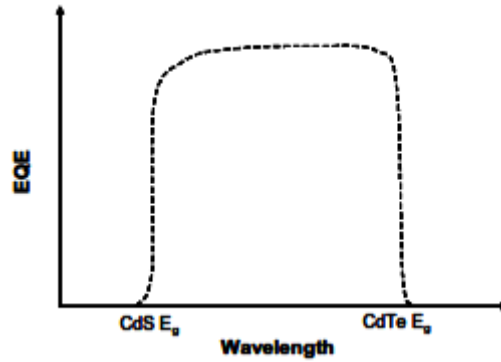


Figure 18. A schematic diagram of idealized EQE curve for CdS-CdTe solar cells [52].

If all the photons of a certain wavelength are absorbed and the resulting carriers are collected, then the QE at that particular wavelength has a value of 100%. The QE for photons with energy below the bandgap is zero. Hence the quantum ideal efficiency has a square shape (Figure 18). However, the QE for most solar cells is reduced because of the effects of recombination, where charge carriers are not able to move into an external circuit. The same mechanisms that affect the collection probability also affect the QE. For example, modifying the cell front surface can affect carriers generated near the surface. And because high-energy (blue) light is absorbed very close to the surface, considerable recombination at the front surface will affect the “blue” portion of the QE.

Similarly, lower energy (green) light is absorbed in the bulk of a solar cell, and a low diffusion length will affect the collection probability from the solar cell bulk, reducing the QE in the green portion of the spectrum. At lower energies QE is rapidly reduced due to passivation of rear cell surface, reduced absorption, and low diffusion length at long wavelengths. Two types of QE of a solar cell are often considered:

1. External QE (EQE) includes the effect of optical losses such as transmission through the cell and reflection of light away from the cell.
2. Internal QE (IQE) refers to the efficiency under exclusion of transmitted or reflected light by the cell. Only the absorbed portion of light can generate charge carriers that can generate current.

The band gap structure in a semiconductor device introduces wavelength dependent absorptivity. A photon with energy larger than the band gap is typically absorbed by the material, while a photon with energy smaller than the band gap is not. The absorbed photon creates an electron-hole pair charge, which leads to creation of electricity. To determine a device’s QE, one must know the power reaching the cell and it’s produced current at each wavelength.

2 EXPERIMENTAL

2.1 Fabrication and characterization of CBD CdS and CdS-CdTe solar cells

2.1.1 Cleaning of substrates

Soda-lime glass substrates were properly cleaned prior to deposition. Velleman digital ultrasonic bath was used to apply ultrasound to substrates in various cleaning solutions. The cleaning procedure consisted of applying ultrasound to substrates submerged in dilute hydrochloric acid, deionized water, acetone, ethanol and deionized water in the given sequence. In between ultrasonic treatment substrates were flushed with deionized water. After proper cleaning, substrates were stored in deionized water.

2.1.2 Deposition of CdS thin films by CBD

CBD technique (Figure 7) was applied to obtain CdS thin film on previously cleaned glass substrates with a 25 mm x 25 mm size. For deposition two glass substrates were immersed back to back on a holder into a covered deposition bath with 180 ml of solution. The composition of the solution (Table 1) was varied by the change of ammonia concentration for different pH values. The pH values were measured at room temperature for each case. When the deposition bath temperature reached 85 °C the final component thiourea (TU) was added into the deposition solution. All the depositions of CdS thin films were done at constant temperature (85 °C) and constant speed of magnetic stirring (500 rpm) in order to guarantee an ideal mixing of the solution.

Table 1: Composition of CBD solution at different pH values

	pH 8.7	pH 9.5	pH 10.0	pH 10.4
CdSO₄	0.001 M	0.001 M	0.001 M	0.001 M
NH₄SO₄	0.03 M	0.03 M	0.03 M	0.03 M
NH₄OH	0.01 M	0.075 M	0.25 M	0.7 M
Thiourea	0.01 M	0.01 M	0.01 M	0.01 M
NH₄Cl	0.001 mM	0.001 mM	0.001 mM	0.001 mM

Depositions were conducted in a manner of sequences, the length of one deposition varied from 10 minutes up to 30 minutes. Overall deposition time for different experiments varied from 60 minutes to 360 minutes. The purpose of changing the deposition times was to achieve the same film thickness at different pH values of solution and also to prevent the CdS growth from bulk of the solution. In between depositions, substrates with CdS thin film were rinsed with distilled water to remove loose particles.

After deposition all CdS thin films were vacuum dried in a closed quartz tube (Figure 19) at 120 °C. The temperature was slowly increased and then kept constant for an hour.

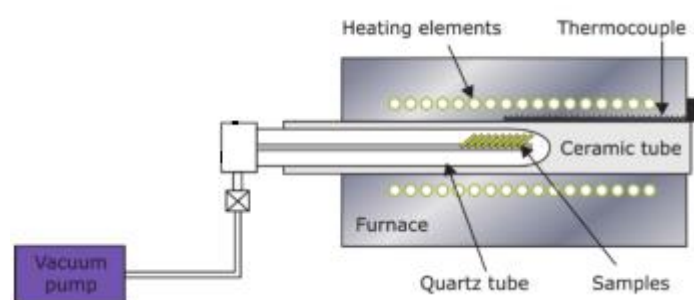


Figure 19. Scheme of vacuum drying setup [45].

Vacuum drying removes most of the secondary phases of water, hydroxides and organic impurities. After this step, the so-called as deposited CdS films were characterized by different techniques.

2.1.3 Fabrication of CdS-CdTe solar cell

For CdS-CdTe solar cell fabrication 100 nm thick CdS thin films were deposited via previously discussed CBD technique on FTO/glass substrates at different solution pH values: 8.7, 9.5, 10.0, 10.4. For solar cell application, intermediate cleaning between deposition sequences was applied – substrates were immersed in triethanolamine (TEA) solution for 5 minutes in ultrasonic bath after which rinsing with distilled water as applied again. This procedure was applied in order to remove poorly adhered CdS particles from the film.

After that, a CdTe layer of 3-4 μm thickness was deposited by closed space sublimation (CSS) at source temperature of 610 °C and substrate temperature of 500 °C. CSS was followed by soaking in CdCl₂ solution, thermal treatment in air at 420 °C, NP etching and deposition of gold back contact by evaporation. For current-voltage and quantum efficiency characterizations large solar cell was scribed into cells of 5mm x 5mm dimension.

2.1.4 Characterization of CdS thin films and CdS-CdTe solar cells

Surface morphology of CdS films was examined by high resolution SEM apparatus (Zeiss Merlin) at an operating voltage of 0.9 kV. The elemental composition of films was determined by means of EDX analysis, using the Bruker EDX-XFlash 6/30 detector with the PB-ZAF standard less mode with a measurement error of ~ 1.0 at. %. Crystallographic investigations were performed using the XRD technique. The measurements were made in the Bragg–Brentano (θ – 2θ) geometry by the Rigaku Ultima IV diffractometer with Cu-K α radiation. Crystallite size, lattice constant and interplanar distance were computed by the PDXL software (Version 1.4.0.3) on the Rigaku system. The crystallite size was calculated using the Debye–Scherrer method and a Scherrer’s constant of 0.94. The optical characteristics were measured in the wavelength range of 200–1500 nm on the Jasco V-670 UV–vis–NIR spectrophotometer equipped with an integrating sphere. The resistivity, charge carrier concentration and mobility were measured at room temperature using MMR’s Variable Temperature Hall System and a Hall and van der Pauw controller H-50. The contact material (indium) for electrical measurements was evaporated through mica mask, which had openings for four-point contact van der Pauw geometry. The resistivities were calculated for thickness of ~ 300 nm which were estimated from SEM analysis.

Performance of the CdS–CdTe solar cells was characterized by current-voltage (J–V) and external quantum efficiency (EQE) measurements. J–V curves were measured under AM1.5 (room temperature, 100 mW/cm^2) conditions using the four-point-probe technique on the AUTOLAB PGSTAT 30 and Oriel class A solar simulator 91159A. The EQE was measured in the spectral region of 300–1000 nm using a computer controlled SPM-2 monochromator (Carl Zeiss-Jena) and a 300 W Xe lamp as the excitation light source. The disperse light from the Xe lamp incident on the solar cell as monochromatic light was optically chopped at 30 Hz.

3 RESULTS AND DISCUSSION

3.1 Properties of CBD CdS thin films

SEM surface images of CBD CdS thin films are presented in Figure 21. Almost all CBD CdS films cover uniformly the underlying glass substrate after one hour of deposition, an exception being the case of deposition at 10.4 pH (Figure 21). At such a high pH value the CdS grains do not manage to coalesce and to cover uniformly the underlying glass substrate. Even by increasing the deposition time from 1 to 2 hours (Figure 20) we obtained CdS films composed of large separated grains that do not cover completely the glass substrate.

The thickness is practically the same (from 243 to 290 nm) for all the films obtained with the deposition time being one hour at different pH values, except for the film obtained at 9.5 pH which is almost twice thicker (438 nm) in comparison to other CdS films (Table 2). This indicates that the film growth rate is fastest with deposition solution pH value 9.5 meaning that the growth mechanism also differs.

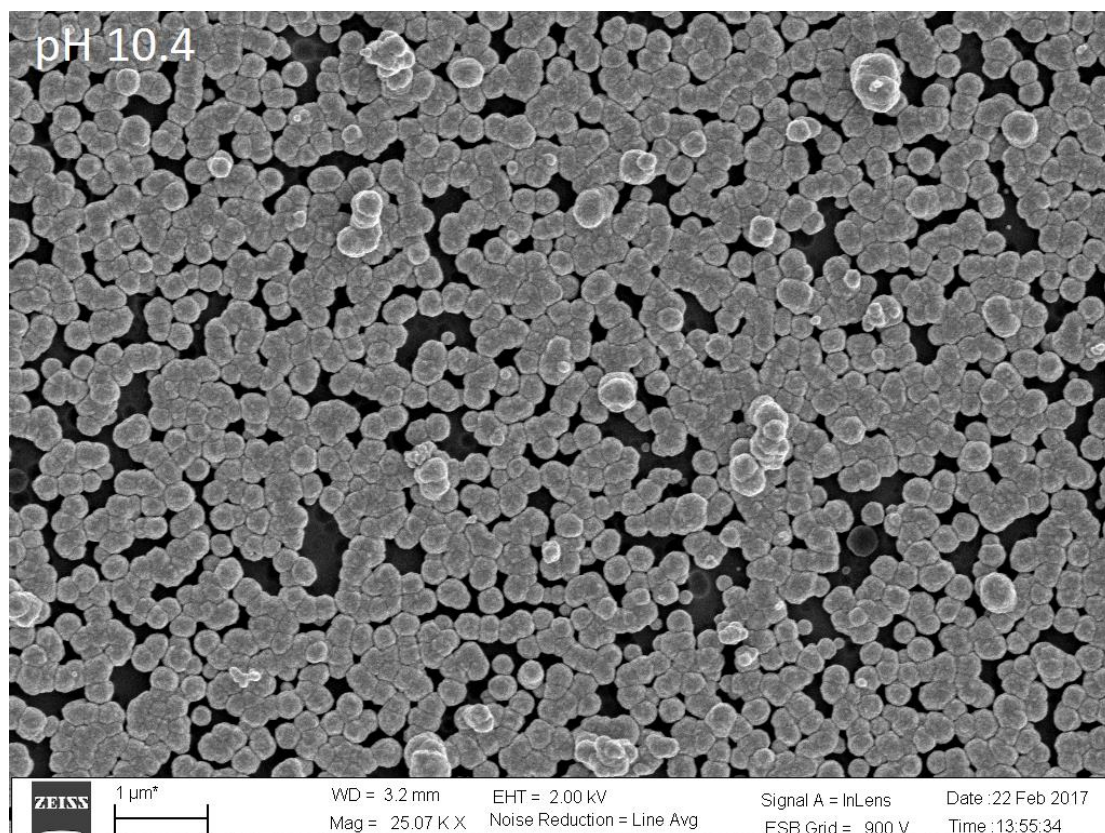


Figure 20. SEM image of CdS thin film obtained at pH 10.4 for deposition time of 2 hours

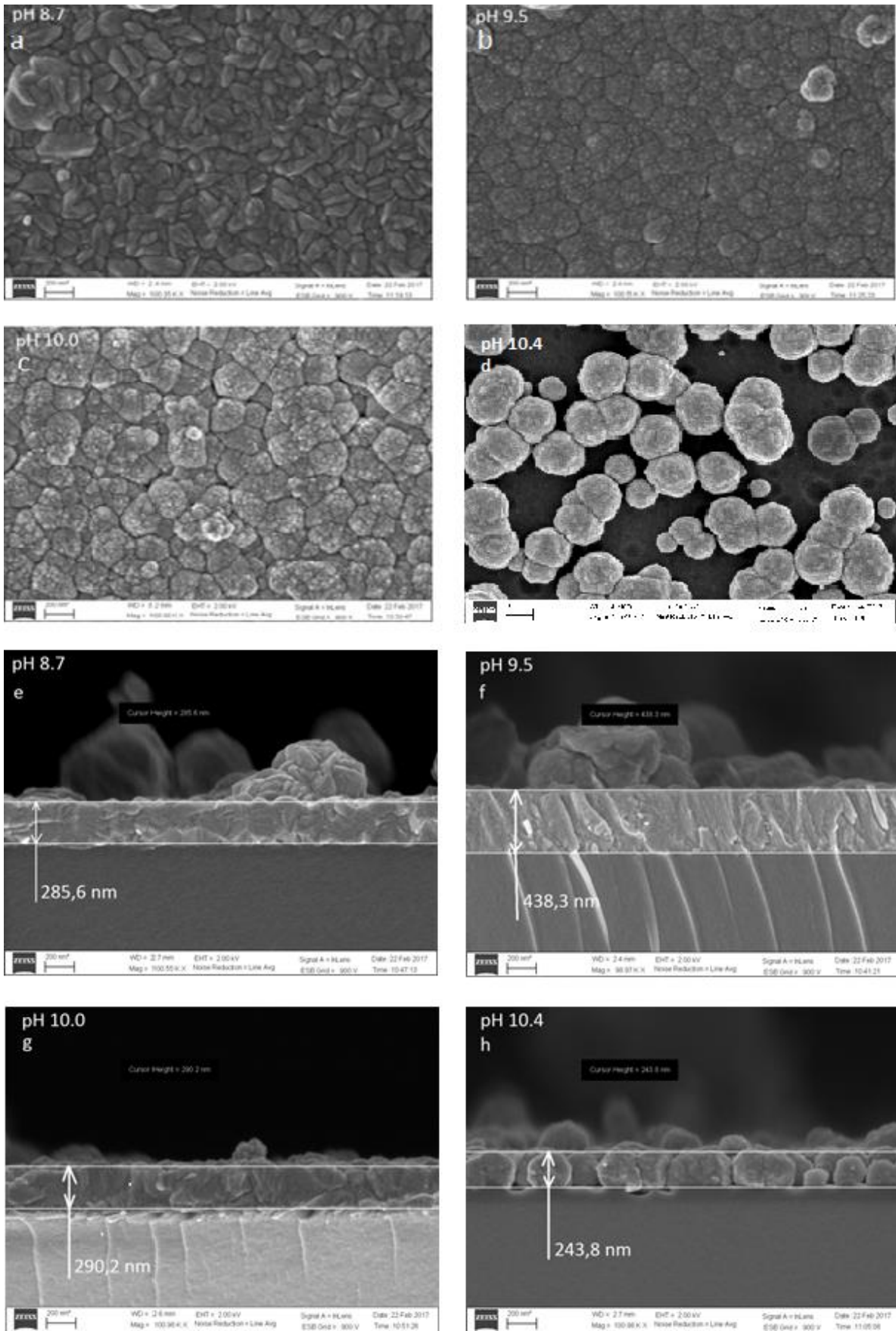
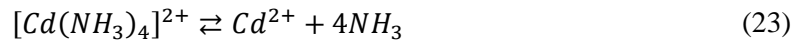


Figure 21. SEM surface view (a-d) and cross sectional image (e-h) of CdS thin films deposited for one hour at different pH values: a, e) 8.7 pH; b, f) 9.5 pH; c, g) 10.0 pH; d, h) 10.4 pH.

The growth mechanism of the CBD CdS films is affected by the value of pH since the change of OH⁻ concentration shifts equilibrium of reactions in the solution. The main reason for formation of heterogeneous CdS crystals is the fact that Cd²⁺ and S²⁻ ions are slowly generated by decomposition of cadmium complex and by hydrolysis of thiourea (2), (3). The maximum concentrations of the ions are governed by the solubility product, K_{sp} (21), of solid CdS.

$$K_{sp} = [Cd^{2+}][S^{2-}] \quad (21)$$

Thiourea decomposes in alkaline solution and based on the equilibria, according to equations (2) and (3), at lower pH values less sulfide ions are formed and vice versa. On the other hand cadmium ions are complexed by ammonium (23) and bound to hydroxide (22), meaning that higher pH value reduces the concentration of free cadmium ions in the solution.



A short scheme (25) shows how the free cadmium and sulfide ion concentrations are affected by the increase of pH in the solution and vice versa (26).



According to this, it seems that in a deposition solution with pH value of 9.5 the concentration of hydroxide ions is optimum for producing similar concentrations of sulfide and cadmium ions in the solution. Such an equilibria of the sulfur and cadmium ions concentration at 9.5 pH assures the fastest growth of CdS thin film whereas lower and higher pHs of the deposition solution the growth is slowed down.

In addition, when the value of solution pH increases from 8.7 to 10.4 we observe an increase in the grain size of CdS thin films from 180 nm up to 300 nm (Table 2). At the same time the grain shape is changed from “beanlike” to spherical, respectively (Figure 21).

When analyzing the elemental composition of CdS thin film by means of EDX, a special attention was paid to the oxygen-containing species in the CdS thin film as a function of solution pH since it is connected to the aim of this master thesis - to study how the pH of solution influences the presence of hydroxide impurities which will be suggested by the oxygen content [9]. From Table 2 it can be seen that all our CdS thin films are S-deficient and we believe that this is caused by the hydroxyl group incorporation on the sulfur site in the CdS crystalline lattice.

Table 2. Thickness, grain size and elemental composition of CBD CdS thin films deposited at different pH values.

pH	8.7	9.5	10.0	10.4
Thickness, nm	285	438	290	243
Grain size, nm	180	180	245	300
[Cd], at. %	52	50	52	52
[S], at. %	41	41	42	43
[O], at. %	7.7	9.2	5.9	4.2

As the pH value is raised from 8.7 up to 10.4 the films keep the same stoichiometry whereas the atomic concentration of oxygen decreases from 7.7 at.% down to 4.2 at.% (Table 2). Similarly to the previously discussed microstructural properties, the CdS thin film deposited at 9.5 pH represents an exception of the tendency and shows the highest content of oxygen impurities (9.2 at.%). We suppose that this is due to the fastest growth of CdS at this solution pH that a larger amount of hydroxide species to be incorporated from the deposition solution (Table 2).

This incorporation, which was previously thoroughly analyzed by X-ray photoelectron spectroscopy [15], is supported here by our XRD analysis (Figure 22, Table 3).

With increasing value of pH, the crystalline structure of CdS thin film changes from multiple orientation to single orientation (Figure 22) with improvement of crystallinity at 9.5 and 10.0 pH values. Moreover, if at low pH values of solution (8.7 pH and 9.5 pH) the deposited CdS thin films have a hexagonal structure, at values higher than 10.0 pH the crystalline structure of CdS re-orientates itself to cubic structure (Table 3). Highest value of pH (10.4) in the deposition solution brings back the disperse structure in the CBD CdS thin film which is described by decreased crystallinity and multiple orientation structure (Figure 22). Taking into account that the incorporated hydroxide impurity in CdS is bound to Cd and that crystalline lattice of Cd(OH)₂ is hexagonal [11], we believe that the high presence of hydroxide impurities at low pH values (Table 2) forces the crystalline lattice of CdS to grow hexagonally. On the other hand, when our CBD CdS thin films contain less hydroxide impurities the CdS lattice re-arrange itself into a stable cubic structure. This assumption is supported by the parameters of crystalline lattice and interplanar distance.

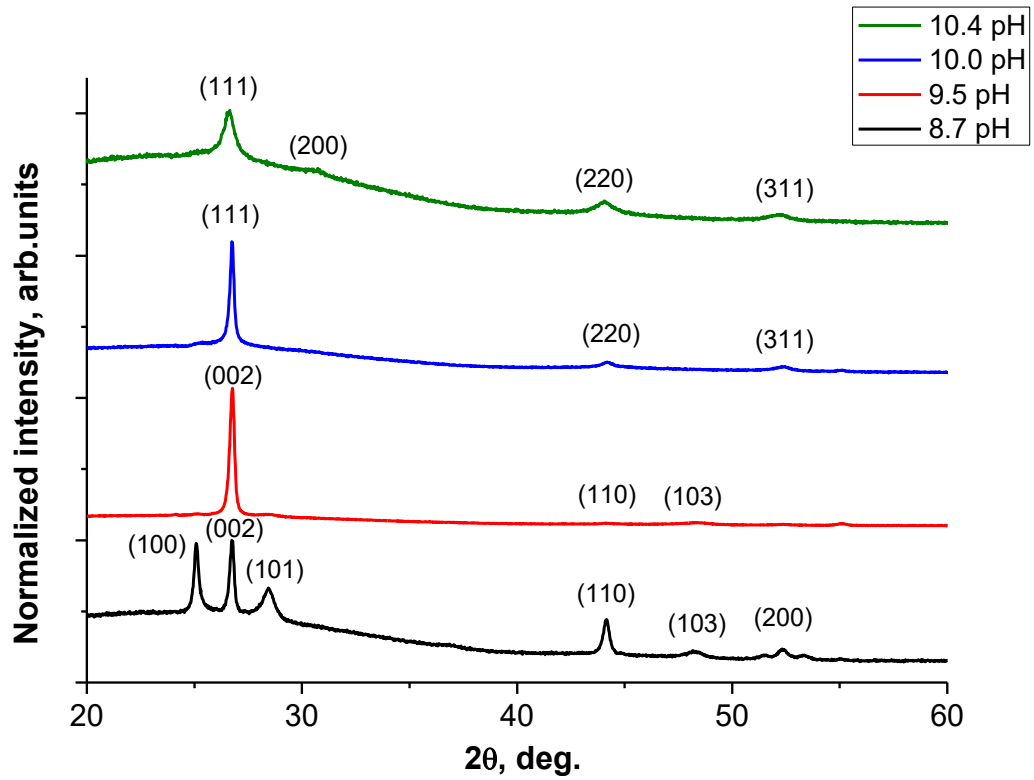


Figure 22. XRD patterns of CBD CdS thin films deposited at different values of solution pH.

Table 3. Interplanar distance (d), and lattice parameters (a , c) calculated for the main XRD peak of CdS thin films deposited at different pH values.

pH	Main peak	2 θ , deg.	d , Å	Ref. 2 θ , deg. [53] [54]	Ref. d , Å [53] [54]	a , Å	c , Å
8.7	(002)	26.752	3.329	26.830	3.321	4.10	6.66
9.5	(002)	26.760	3.328	26.830	3.321	4.08	6.65
10.0	(111)	26.742	3.331	26.460	3.370	5.77	-
10.4	(111)	26.662	3.341	26.460	3.370	5.88	-

At higher pH values we observe an increase in the interplanar distance (Table 3). This is because at higher pH values there is less incorporated OH impurities (Table 2) on the sulfur site and since the covalent radius of OH group (96 pm) is smaller than the covalent radius of sulfur itself (105 pm) it causes relaxation or stretching of the CdS lattice [55]. Following the same logic, also the lattice parameter increases for cubic structure when the content of oxygen decreases and for hexagonal structure the same tendency can be observed.

The optical band gap values of CBD CdS thin films confirm that the characteristics of Cd(OH)₂ dictate the properties of CdS. The general trend of band gap value is a decrease from

2.43 eV to 2.31 eV corresponding to a raise in the value of solution pH from 8.7 up to 10.4 and is in close correlation with oxygen content from previously shown EDX data (Table 2). This tendency is in agreement with Yucel et al. study that showed that the band gap of CdS is decreased when a higher pH is applied in the deposition process [56]. Again, CdS thin films with a higher content of oxygen impurities have a higher band gap and vice versa (Figure 23) and we connect it to the high band gap of incorporated Cd(OH)₂ [57]. Still, compared to Yucel et al. work [56], in our case the band gap values are lower due to less concentrated solution, higher Cd:S ratio and lower pH values.

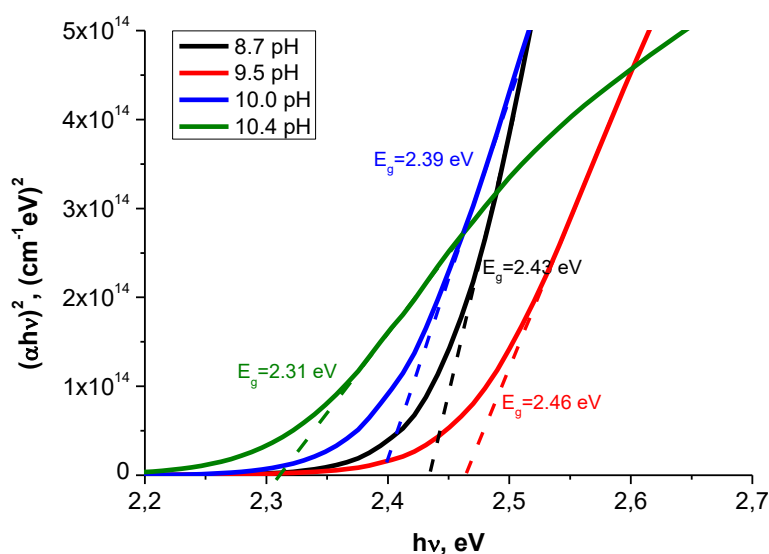


Figure 23. Tauc's plots and band gap values of CBD CdS thin film deposited at different pH values of solution.

When coming to electrical properties, resistivity and sheet resistance for the films were measured only for CdS films deposited at pH values 8.7, 9.5 and 10.0 (Table 4). The film deposited at 10.4 pH is described by a poor coverage of a substrate and unconnected grains; therefore no lateral charge transport was possible to register. CdS deposited at 9.5 pH has the smallest resistivity and sheet resistance. Due to device limitations of the Hall effect technique charge carrier mobility ($3.39 \text{ cm}^2/\text{Vs}$) and density ($1.71 \cdot 10^{19} \text{ cm}^{-3}$) could only be measured for this sample.

Table 4. Electrical properties of CdS thin films obtained at different pH of deposition solution

pH	8.7	9.5	10.0
R_{sheet}, Ω	$2.80 \cdot 10^7$	$5.00 \cdot 10^3$	$1.80 \cdot 10^6$
Resistivity, $\Omega \cdot \text{cm}$	$2.94 \cdot 10^2$	$1.08 \cdot 10^{-1}$	$3.87 \cdot 10^1$

To summarize, in this study we managed to influence the content of hydroxide species by changing the value of pH solution. We decreased the oxygen concentration from 7.7 at.% down to 4.2 at.% when raising the value of solution pH from 8.7 up to 10.4 (Table 2). However, the CdS film obtained at 10.4 pH is also described by poorest substrate coverage. Such microstructure of this CdS film makes its application as a buffer layer almost impossible. Therefore, for solar cell application we tested only CdS thin films deposited at three pH values: 8.7, 9.5, and 10.0.

3.2 Properties of CdS/CdTe solar cells

Figure 24a shows the current-voltage (J–V) characteristics of CdS–CdTe solar cells with ~100 nm thick CdS films obtained at different values of solution pH: 8.7, 9.5, and 10.0. The photoelectric performance of these solar cells is shown in Table 5.

The highest performance is shown by the solar cell with CdS film deposited at 10.0 pH. An important reason for this improvement might be the lowest concentration of oxygen containing species, larger grains of CdS (Table 2), and less interface defects between this CdS film and CdTe absorber that has much larger grain size. Solar cell with CdS deposited at 8.7 pH show lowest solar cell parameters (Table 5) due to smallest grain size of CdS film (Table 2) and therefore more interface defects. When compared to the cells with CdS deposited at pH 9.5 and 10.0, the grain size of only 180 nm for CdS deposited at 8.7 pH implies a faster interdiffusion at the CdS/CdTe junction interface in the process of CdCl₂ treatment. This interdiffusion appears to be accelerated also by the relatively high oxygen content in this CBD CdS film [45]. Additionally, the resistivity of CdS layer deposited at 8.7 pH is very large and also lowers the devices performance. On the other hand, CdS thin film deposited at pH 9.5 (which has the same grain size) is described by a very large charge carrier density causing the shrinkage of depletion layer and thus reduction of the open circuit voltage of the device. The optimum electrical properties for CdS thin film for solar cell fabrication seem to be at deposition pH value of 10.0 (Figure 24).

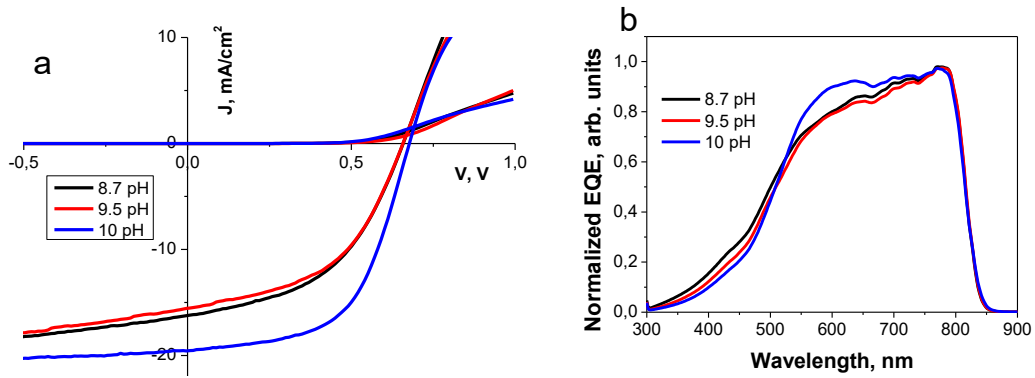


Figure 24. J-V (a) and EQE (b) characteristics of CdS-CdTe solar cells with CBD CdS obtained at different values of solution pH (8.7, 9.5 and 10.0).

Table 5. Photovoltaic parameters of CdS-CdTe solar cells with CBD CdS film obtained at different values of solution pH (8.7, 9.5, and 10.0)

pH	V _{OC} , V	J _{SC} , mA/cm ²	FF, %	η, %
8.7	660	16.1	48	5.1
9.5	660	15.5	49	5.0
10.0	680	19.5	57	7.6

These conclusions are supported by simultaneous changes of the EQE dependencies (Figure 24b) in the wavelength region of 300-700 nm. The solar cells with CdS deposited at 8.7 and 9.5 pH exhibit slightly higher EQE response in the mentioned wavelength region probably because of the thinning of CdS as a result of intermixing at the CdTe-CdS interface [18]. Although this enhancement is beneficial for buffer transmission, non-uniform CdS consumption may lead to the formation of parallel junctions between the absorber and FTO front contact, and hence to the reduction of solar-cell performance (Table 5). Based on these arguments it is clear that solar cell that uses CdS with larger grains obtained at pH value of 10.0 exhibits the best EQE response implying better collection efficiency.

4 CONCLUSIONS

A systematic study of changes in the properties of CBD CdS thin films deposited at pH values of 8.7, 9.5, 10.0 and 10.4 was carried out in order to understand the physico-chemical mechanisms of the deposition process and influence on the properties of superstrate CdS-CdTe solar cells.

The results are as follows:

1. The changes of pH from 8.7 to 10.4 in the deposition solution were achieved by changing ammonia concentration from 0.01 M to 0.7 M in the presence of 0.03 M buffer $(\text{NH}_4)_2\text{SO}_4$.
2. An increase of pH value from 8.7 up to 10.4 generates an increase of grain size from 180 nm to 300 nm whereas the coverage and uniformity of the film is damaged at 10.4 pH. In addition, with increasing the pH value of solution the crystalline structure of CdS thin films is transformed from hexagonal (002) towards cubic (111) with increasing of interplanar distance.
3. We managed to decrease the amount of oxygen impurities in CBD CdS thin films from 7.7 at.% to 4.2 at.% by means of increasing pH values from 8.7 up to 10.4. The band gap changes from 2.46 eV to 2.31 eV and are in close correlation with concentration of oxygen content determined by EDX which we connected with the amount of OH impurities incorporated in the CdS lattice.
4. We claim that all the changes in the film properties are generated by the changing of growth mechanism of CdS in result of pH modification. Due to different equilibria of Cd^{2+} and S^{2-} ion concentrations in the deposition solution the fastest CdS growth occurs at pH value of 9.5 while the amount of incorporated hydroxides is inversely proportional to the pH value of the solution.
5. In solar cell application, by using CBD CdS films deposited at 8.7 pH up to 10.0 pH values, we managed to increase the solar cell efficiency from 5.1 % up to 7.6 %. Such an improvement of CdS-CdTe solar cell parameters are due to larger grain size of CdS film as well as decreased amount of oxygen containing species at higher pH values.

ABSTRACT

High quality CdS thin films are of great interest in the thin film photovoltaic community due to their application as a buffer layer in thin film solar cells like CIGS, CdTe and kestersite. CdS impurities like oxygen and hydroxide impact the electrical, optical and structural properties of CdS film, which may cut the performance of CdTe, CIGS or CZTS devices. One of the possibilities to control the hydroxide content in CBD CdS lattice is the pH modification of the deposition solution. In the present work we study the effect of solution pH on the hydroxide content and the growth mechanism in CBD CdS thin film. Also changes in structural, optical and electrical properties are given as function of deposition solution pH. We noticed that a change in the pH from 8.7 to 10.4 gives raise to major variations in CdS properties measured by X-ray diffraction, UV-vis spectroscopy, energy-dispersive X-ray spectroscopy, scanning electron microscopy, Hall and van der Pauw techniques. At low pH values (8.7, 9.5 and 10.0) CdS films are dense and uniformly cover the glass substrates. The grain sizes of these films are similar of 180 nm for films obtained at 8.7 pH and 9.5 pH and increased to 243 nm for pH value of 10.0. The rate of film growth is doubled for CdS film deposited at 9.5 pH which is caused by optimal Cd^{2+} and S^{2-} concentrations in the deposition solution. At higher pH value (10.4) the films become porous and have a grain size of 300 nm. The crystalline structure of CdS thin film obtained at 8.7 - 10.4 pH changed from (002) hexagonal to (111) cubic, respectively. The influence of CdS films deposited at different pH values on the device performance is shown for superstrate CdS-CdTe solar cells. Due to less hydroxide impurities and larger CdS grains at higher pH values of deposition solution the photovoltaic parameters of CdS-CdTe solar cells were improved and the efficiency was raised from 5.1 % up to 7.6%;

KOKKUVÕTE

Päikeseenergeetika kogukondades on huvi kvaliteetsete CdS õhukeste kilede järgi suur. CdS kilesid kasutatakse akna kihina kiletehnoloogiatel põhinevates päikeseplatadeid, mis baseeruvad järgmistel absorberitel: CIGS, CdTe ja kesteriidid. Hapniku ja hüdroksüülrühma lisandid mõjutavad CdS kilede struktuurseid, optilisi ja elektrilisi omadusi, mis omakorda mõjutavad eelmainitud päikeseelementide efektiivsust. Üheks võimaluseks kontrollida hüdroksüülrühma lisandite kogust CdS kiles on muuta keemilise sadestuse vanni pH väärtusi. Käesolevas töös uurisime CBD meetodi lahuse pH mõju CdS kilede kasvu mehhanismile ning hüdroksüüli lisandile. Samuti uurisime struktuursete, optiliste ja elektriliste omaduste muutust lahuse pH võtmes. Uurisime CdS õhukeste kilesid röntgen difraktomeetria, UV-nähtava valguse spektroskoopia, energia hajuvusspektroskoopia, skanneeriva elektronmikroskoopia ja Halli ning van der Pauw tehnikatega ning täheldasime suuri muutusi kilede omadustes sadestuslahuse pH väärtuste muutumisel 8.7 kuni 10.4. Madalamatel pH väärtustel (8.7, 9.5 ja 10.0) sadestatud kiled on tihedad ja katavad substraati ühtlaselt. 8.7 ja 9.5 pH väärtuste juures sadestatud kilede tera suurused on ühesugused (180 nm), kuid pH 10.0 juures sadestatud kile tera suurus on 243 nm. Samuti on kile kasvu kiirused erinevad - pH 9.5 korral on kasvu kiirus suurim. Kõrge kasvukiirus tagati optimaalse vabade Cd^{2+} ja S^{2-} ionide kontsentratsiooniga lahuses. pH väärtustel 10.4 muutuvad kiled poorseks ning terade suurus kasvab veelgi kuni 300 nm. Kristallivõre struktuur muutus lahuse pH tõusuga heksagonaalsest (002) kuubiliseks (111). Uurisime ka CdS õhukese kile omaduste mõju pööratud struktuuriga CdTe põhineva päikeseelemendi efektiivsusele. Leidsime, et tõstes sadestamislahuse pH väärtust 8.7 kuni 10.0 vähenes hüdroksüülrühma lisandi kogus ning suurenes terade suurus, mis tagasid päikeseelemendi efektiivsuse tõusu 5.1% kuni 7.6%.

REFERENCES

- [1] A. Luque ja S. Hegedus, Handbook of Photovoltaic Science and Engineering, 2nd edition, Chichester, UK: John Wiley & Sons Ltd, 2010.
- [2] G. X. Liang, P. Fan, Z. H. Zheng, J. T. Luo, D. P. Zhang, C. M. Chen ja P. J. Cao, „Room-temperature preparation and properties of cadmium sulfide thin films by ion-beam sputtering deposition,“ *Applied Surface Science*, kd. 273, pp. 491-495, 2013.
- [3] B. Gosh, M. Das, P. Banerjee ja S. Das, „fabrication of vacuum-evaporated SnS/CdS heterojunction for PV applications.,“ *Sol. Energy Mater. Sol. Cells*, kd. 92, pp. 1099-1104, 2008.
- [4] A. S. Baranski, W. R. Fawcett ja A. C. McDonald, „The mechanism of electrodeposition of cadmium silfide on inert metals from dimethylsulpoxide solution,“ *J. Electroanal. Chem. Interfacial Electrchem.*, kd. 160, pp. 271-287, 1984.
- [5] A. Yadav, M. Barote ja E. Masumdar, „Studies on nanocrystalline cadmium sulphide thin films deposited by spray pyrolysis,“ *Solid State Science*, kd. 12, pp. 1173-1177, 2010.
- [6] O. Isaiah ja L. Oladeji, „Optimization of chemical bath deposited cadmium sulfide thin films,“ *J. Electrochem. Soc.*, kd. 144, pp. 2342-2346, 1997.
- [7] S. Soundeswaran, O. S. Kumar ja R. Dhanasekaran, „Effect of Ammonium Sulphate on Chemical Bath Deposition of CdS Thin Films,“ *Materials Letters*, kd. 58, pp. 2381-2385, 2004.
- [8] G. Hodes, Chemical solution deposition of semiconductor films, 2002.
- [9] R. Ortega-Borges ja D. Lincot, „Mechanism of Chemical Bath Deposition of Cadmium Sulphide Thin Films in the Ammonia-Thiourea System,“ *J. Electrochem. Soc.*, kd. 140, pp. 3464-3473, 1993.
- [10] I. Kaur, D. K. Pandya ja K. L. Chopra, „Growth Kinetics and Polymorphism of Chemically Deposited CdS Films,“ *J. Electrochem. Soc.*, kd. 127, pp. 943-948, 1980.
- [11] A. Kylner, A. Rockett ja L. Stoly, „Oxygen in solution growth CdS films for thin iflm solar cells,“ *Solid State Phenom.*, Kd-d. % 1/% 251-52, pp. 533-540, 1996.
- [12] N. S. Kozhevnikova, A. A. Rempel, F. Hergert ja A. Magerl, „Structural Study of the Initial Growth of Nanocrystalline CdS Thin Films in a Chemical Bath,“ *Thin Solid Films*, kd. 517, pp. 2586-2589, 2009.
- [13] S. Lee, E. S. Lee, T. Y. Kim, J. S. Cho, Y. J. Eo, J. H. Yun ja A. Cho, „Effects od Annealing Treatment on CdS/GIGS Thin Films Solar Cells Depending on Different CdS Deposition Temperatures,“ *Sol. Energy Mater. Sol. Cells*, kd. 141, pp. 299-308, 2015.
- [14] M. J. D. Low ja A. M. Kamel, „The Thermal Decomposition of Cadmium Hydrozide,“ *J. Phys. Chem.*, kd. 69, pp. 450-457, 1965.

- [15] N. Maticiuc, A. Katerski, M. Danilson, M. Krunkls ja J. Hiie, „XPS study of OH impurity in solution processed CdS thin films,“ *Solar Energy Materials & Solar Cells*, kd. 160, pp. 211-216, 2017.
- [16] N. Maticiuc, J. Hiie, V. Mikli, T. Potlog ja V. Valdna, „Structural and Optical Properties of Cadmium Sulfide Thin Films Modified by Hydrogen Annealing,“ *Materials Science in Semiconductor Processing*, kd. 26, pp. 169-174, 2014.
- [17] N. Maticiuc, J. Hiie, T. Potlog, V. Valdna ja A. Gavrilov, „Influence of Annealing in H₂ Atmosphere on the Electrical Properties of Thin Film CdS,“ *Mater. Res. Soc. Symp. Proc.*, kd. 1324, 2011.
- [18] N. Maticiuc, N. Spalatu, V. Mikli ja J. Hiie, „Impact of CdS annealing atmosphere on the performance of CdS-CdTe solar cell,“ *Applied Surface Science*, kd. 350, pp. 14-18, 2015.
- [19] M. Jonathan, CdTe solar cells: growth phenomena and device performance, Doctoral thesis, Durham University, 2008.
- [20] M. V. Madsen, „www.plasticphotovoltaics.org,“ [Vörgumaterjal]. Available: <http://plasticphotovoltaics.org/lc/lc-solarcells/lc-introduction.html>.
- [21] „Press release: Solar Frontier Achieves World Record Thin-Film Solar Cell Efficiency: 22,3%“.
- [22] M. A. Green, K. Emery, Y. Hishikawa, W. Warta ja E. Dunlop, „Solar cell efficiency tables (version 46),“ *Prog. Photobolt: Res. Appl.*, kd. 23, pp. 805-8012, 2015.
- [23] F. Meillaud, M. Boccard, G. Bugnon, M. Despeisse, S. Hänni, F. J. Haug, J. Persoz, J. W. Schüttauf, M. Stuckelberger ja C. Ballif, *Materials Today*, pp. 378-384, 2015, September.
- [24] J. Poortmans ja V. Arkhipov, *Thin Film Solar Cells Fabrication, Characterization and Applications*, Leuven: John Wiley & Sons, 2006.
- [25] „solars-china.com,“ China Solar, [Vörgumaterjal]. Available: <http://www.china-calculators.com/solar08.html>.
- [26] D. L. Staebler ja C. R. Wronski, *Appl. Phys. Lett.*, kd. 31, pp. 292-294, 1977.
- [27] H. Heriche, Z. Roubah ja N. Bouarissa, „New ultra thin CIGS structure solar cells using SCAPS simulation program,“ *International Jurnal of Hydrogen Energy*, kd. 42, nr 15, pp. 9525-9532, 2017.
- [28] B. L. Olivia-Chatelain ja A. R. Barron, „An Introduction to Solar Cell Technology,“ [Vörgumaterjal]. Available: <http://cnx.org/contents/3QU3ovtd@1/An-Introduction-to-Solar-Cell->.
- [29] M.-H. Yeh, H.-R. Hsu, K.-C. Wang, S.-J. H. G.-H. Chen ja H.-S. Chen, „Toward low-cost large-area CIGS thin film: Compositional and structural variations in sequentially electrodeposited CIGS thin films,“ *Solar Energy*, kd. 125, pp. 415-425, 2016.
- [30] X. Mathews, G. W. Thompson, V. P. Singh, J. C. McClure, S. Velumani, N. R. Mathews ja P. J.

- Sebastian, *Solar Energy Materials and Solar Cells*, kd. 76, pp. 293-303, 2003.
- [31] K. Mitchell, A. L. Fahrenbruch ja R. H. Bube, *J. Appl. Phys.*, kd. 48, pp. 1977-1978, 1977.
- [32] A. M. Acevedo, *Sol. Energy Mater. Sol. Cells*, kd. 90, pp. 2213-2220, 2006.
- [33] R. W. Birkmire ja E. Eser, *Annu. Rev. Mater. Sci.*, kd. 27, pp. 625-653, 1997.
- [34] N. Romeo, A. Bosio ja A. Romeo, *Sol. Energy Mater. Sol. Cells*, kd. 94, pp. 2-7, 2010.
- [35] A. M. Acevedo, *Sol. Energy Mater. Sol. Cells*, kd. 90, pp. 678-685, 2006.
- [36] V. Avrutin, N. Izyumskaya ja H. Morkoc, *Superlattices Microstruct.*, kd. 49, pp. 337-364, 2011.
- [37] B. E. McCandless, I. Youm ja R. W. Birkmire, „Optimization of Vapor Post-deposition Processing for Evaporated CdS/CdTe Solar Cells,“ *Prog. Photovolt. Res. Appl.*, kd. 7, pp. 21-30, 1999.
- [38] X. Mathew, J. S. Cruz, D. R. Coronado, A. R. Millan, G. C. Segura, E. R. Morales, O. S. Martinez, C. C. Garcia ja E. P. Landa, „CdS thin film post-annealing and Te-S interdiffusion in a CdTe/CdS solar cell,“ *Solar Energy*, kd. 86, nr 4, pp. 1023-1028, 2012.
- [39] B. Mereu, G. Sarau, E. Pentia, V. Draghi, M. Lisca, T. Botila ja L. Pintilie, „Field effect transistor based on nanometric thin film CdS films,“ *Mat. Sci. Eng.*, kd. 109, pp. 260-263, 2004.
- [40] M. Antoniadou, V. Daskalakis, N. Balis, D. Kondarides, C. Kordulic ja P. Lianos, „Photocatalysis and photoelectrocatalysis using (CdS-ZnS)/TiO₂ combined photocatalysis,“ *Appl. Catal. B: Environ.*, kd. 107, pp. 188-196, 2011.
- [41] R. Williams ja R. Bube, „Photoemission in the photovoltaic effect in cadmium sulfide crystals,“ *J. Appl. Phys.*, kd. 31, pp. 968-978, 1960.
- [42] A. Oliva, O. Solis-Canto, R. Castro-Rodriguez ja P. Quintana, „Formation of the band gap energy on CdS thin films grown by two different techniques,“ *Thin Solid Films*, kd. 391, pp. 28-35, 2001.
- [43] X. L. Tong, D. S. Jiang, Z. M. Liu, M. Z. Luo, Y. Li, P. X. Lu, G. Yang ja H. Long, „Structural characterization of CdS thin films on quartz formed by femtosecond pulsed laser deposition at high temperature,“ *Thin Solid Films*, kd. 516, pp. 2003-2008, 2008.
- [44] B. Ghosh, B. K. Singh, P. Banerjee ja S. Das, „Nucleation and growth of CBD. CdS thin films on ultrathin aluminium layers and annealing induced doping,“ *Optik*, kd. 127, pp. 4413-4417, 2016.
- [45] N. Maticiuc, *Mechanism of Changes in the Properties of Chemically Deposited CdS Thin Films Induced by Thermal Annealing*, Tallinn: TUT press, 2015.
- [46] J. A. Garcia-Valenzuela, „Simple Thiourea Hydrolysis or Intermediate Complex Mechanism? Taking Up the Formation of Metal Sulfides from Metal-Thiourea Alkaline Solutions,“ *Comments on Inorganic Chemistry*, kd. 37, pp. 99-115, 2016.
- [47] G. Kitaev, A. Uritskaya ja S. Mokrushin, *Russ. J. Phys. Chem.*, p. 39:1101, 1965.

- [48] R. Jayakrishnan, J. P. Nair, B. A. Kuruvilla, S. K. Kulkarni ja R. K. Pandey, „Characterization and photovoltaic device application of dip-coated and rapid thermal annealed CdS films,“ *J Mater. Sci.*, kd. 7, nr 3, pp. 193-199, 1996.
- [49] Abou-Ras, Kirchartz, Rau, *Advanced Characterization Techniques for Thin Film Solar Cells*, Wiley-VCH, 2011.
- [50] M. Safonova, *SnS Thin Films Deposition by Chemical Solution Method and Characterization*, Tallinn, 2016.
- [51] L. J. v. d. Pauw, *A Method of Measuring the Resistivity and Hall Coefficient on Lamellae of Arbitrary Shape*, Philips Research Reports, 1958.
- [52] A. Mohammed, „CdTe Solar Cells: Key Layers and Electrical Effects,“ *Durham Theses, Durham University*, 2010.
- [53] ICDD file no: 01-074-9665, Bibl.: H. Sowa, *Solid state Sci.* 7. (2005) 73.
- [54] ICDD file no: 01-089-0440, Bibl.: D. Rodic, V. Spasojevis, A. Bajorek, P. J. Onnerund, *Magn. Mater.* 152 (1996) 159.
- [55] B. Cordero, V. Gomez, A. E. Platero-Prats, M. Reves, J. Echeverra, E. Gremades, F. Barragan ja S. Alvarez, „Covalent radii revisited,“ *Dalton Trans.*, pp. 2832-2838, 2008.
- [56] E. Yücel ja O. Sahin, „Effect of pH on the structural, optical and nanomechanical properties of CdS thin films grown by chemical bath deposition,“ *Ceramics International*, kd. 42, pp. 6399-6407, 2016.
- [57] B. Sahin, F. Bayansal, H. M. Cakmak, S. Kahraman ja H. A. Cetinkara, „Effect of heat treatment on the properties of Cd(OH)₂ and CdO films grown by chemical bath deposition,“ *Philosophical Magazine Letters*, kd. 93, pp. 101-108, 2013.
- [58] Ersin Yücel, Osman Sahin, „Effect of pH on the structural, optical and nanomechanical properties of CdS thin films grown by chemical bath deposition,“ *Ceramic international*, 2016.
- [59] J.M. Dona; J. Herrero, „Chemical bath deposition of CdS thin films: An approach to the chemical mechanism through study of the film microstructure,“ *The electrochemical society*, kd. 144, nr 11, 1997.
- [60] T. Dittrich, *Materials Concepts for Solar Cells*, London: Imperial College Press, 2015.
- [61] A. Kylner ja M. Wirde, „A High-Resolution X-ray Photoelectron Spectroscopy Study of Carbon-Nitrogen Impurity in Chemical Bath Deposited CdS Thin Films,“ *Japanese Journal of Applied Physics*, kd. 36, pp. 2167-2175, 1997.
- [62] E. Wiberg ja N. Wiberg, *Inorganic chemistry*, Academic Press, 2001.

ACKNOWLEDGEMENTS

I am thankful to the director of Materials and Environmental Technology Department - Malle Krunk, for giving me this opportunity to work in the laboratory of thin film chemical technologies. I would like to thank my supervisors PhD Natalia Maticiuc and PhD Nicolae Spalatu who have been extremely helpful throughout this work. Also I would like to thank Dr Jaan Hiie for providing many useful explanations and many thanks to Olga Volobujeva for helping out with SEM/EDX measurements.

This work was financially supported by the Estonian Ministry of Education and Research [projects IUT19-4]; the Estonian Centre of excellence in Research [Project TK141].

I would like to express my warmest gratitude towards my family members who have shown great support during my studies in TUT.

Marvin Üürike